J|A|C|S ARTICLES

Published on Web 09/02/2009

A Comparison of 4*f* *vs* 5*f* Metal−Metal Bonds in $(CpSiMe_3)_3M-ECp^*$ (M = Nd, U; E = Al, Ga; $Cp^* = C_5Me_5$): Synthesis, Thermodynamics, Magnetism, and Electronic Structure

Stefan G. Minasian,[†] Jamin L. Krinsky,[*,‡] Jeffrey D. Rinehart,[†] Roy Copping,[§] Tolek Tyliszczak,[||] Markus Janousch,[||,⊥] David K. Shuh,[*,§] and John Arnold[*,†]

Department of Chemistry, University of California, Berkeley, California 94720, Molecular Graphics and Computation Facility, University of California, Berkeley, California 94720, Chemical Sciences Division, Lawrence Berkeley National Laboratory, Berkeley, California 94720, Advanced Light Source, Lawrence Berkeley National Laboratory, Berkeley, California 94720, and Paul Scherrer Institute (PSI), 5232 Villigen-PSI, Switzerland

Received June 4, 2009; E-mail: arnold@berkeley.edu; jamink@berkeley.edu; dkshuh@lbl.gov

Abstract: Reaction of $(CpSiMe_3)_3U$ or $(CpSiMe_3)_3Nd$ with $(Cp^*Al)_4$ or Cp^*Ga ($Cp^* = C_5Me_5$) afforded the isostructural complexes $(CpSiMe_3)_3M-ECp^*$ (M = U, E = Al (**1**); M = U, E = Ga (**2**); M = Nd, E = Al (**3**); M = Nd, E = Ga (**4**)). In the case of **1** and **2** the complexes were isolated in 39 and 90% yields, respectively, as crystalline solids and were characterized by single-crystal X-ray diffraction, variable-temperature ^{1}H NMR spectroscopy, elemental analysis, variable-temperature magnetic susceptibility, and UV−visible−NIR spectroscopy. In the case of **3** and **4**, the complexes were observed by variable-temperature ^{1}H NMR spectroscopy but were not isolated as pure materials. Comparison of the equilibrium constants and thermodynamic parameters ΔH and ΔS obtained by ^{1}H NMR titration methods revealed a much stronger U−Ga interaction in **2** than the Nd−Ga interaction in **4**. Competition reactions between $(CpSiMe_3)_3U$ and $(CpSiMe_3)_3Nd$ indicate that Cp^*Ga selectively binds U over Nd in a 93:7 ratio at 19 °C and 96:4 at −33 °C. For **1** and **3**, comparison of ^{1}H NMR peak intensities suggests that Cp^*Al also achieves excellent U(III)/Nd(III) selectivity at 21 °C. The solution electronic spectra and solid-state temperature-dependent magnetic susceptibilities of **1** and **2**, in addition to X-ray absorption near-edge structure (XANES) measurements from scanning transmission X-ray microscopy (STXM) of **1**, are consistent with those observed for other U(III) coordination complexes. DFT calculations using five different functionals were performed on the model complexes Cp_3M-ECp (M = Nd, U; E = Al, Ga), and empirical fitting of the values for Cp_3M-ECp allowed the prediction of binding energy estimates for Cp^*Al compounds **1** and **3**. NBO/NLMO bonding analyses on Cp_3U-ECp indicate that the bonding consists predominantly of a E→U σ-interaction arising from favorable overlap between the diffuse ligand lone pair and the primarily 7*s*/6*d* acceptor orbitals on U(III), with negligible U→E π-donation. The overall experimental and computational bonding analysis suggests that Cp^*Al and Cp^*Ga behave as good σ-donors in these systems.

Introduction

For generations, synthetic inorganic chemists have developed theories of chemical bonding, magnetism, and materials chemistry through the study of molecular metal−metal bonds.[1] Yet among the abundance of known bonds between metals spanning most of the Periodic Table, relatively few have been reported involving the actinides. Following the first examples of unsupported An−M bonds, which include $Cp_3U-SnPh_3$[2] and a series of U and Th complexes with Fe and Ru reported in the late 1980s,[3] the subject fell into a period of inactivity. Recently, perhaps bolstered by reports of unusual bonding involving the actinides,[4] theoretical investigations enabled by advances in computational resources,[5] and new synthetic methods and starting materials,[6] progress has been made on the study of molecular metal−metal bonding involving the 5*f*-elements.

Formation of new *f*-element metal−metal bonds has been principally achieved through metathesis or by exploiting coordinative unsaturation in starting materials.[7] By the latter strategy,

[†] Department of Chemistry, University of California.
[‡] Molecular Graphics and Computation Facility, University of California.
[§] Chemical Sciences Division, Lawrence Berkeley National Laboratory.
[||] Advanced Light Source, Lawrence Berkeley National Laboratory.
[⊥] Paul Scherrer Institute.

(1) Cotton, F. A.; Murillo, C. A.; Walton, R. A. *Multiple Bonds Between Metal Atoms*, 3rd ed.; Springer Science: New York, NY, 2005.
(2) Porchia, M.; Casellato, U.; Ossola, F.; Rossetto, G.; Zanella, P.; Graziani, R. *Chem. Commun.* **1986**, 1034–1035.
(3) (a) Sternal, R. S.; Brock, C. P.; Marks, T. J. *J. Am. Chem. Soc.* **1985**, *107*, 8270–8272. (b) Sternal, R. S.; Marks, T. J. *Organometallics* **1987**, *6*, 2621–2623. (c) Sternal, R. S.; Sabat, M.; Marks, T. J. *J. Am. Chem. Soc.* **1987**, *109*, 7920–7921.
(4) (a) Diaconescu, P. L.; Arnold, P. L.; Baker, T. A.; Mindiola, D. J.; Cummins, C. C. *J. Am. Chem. Soc.* **2000**, *122*, 6108–6109. (b) Castro-Rodriguez, I.; Nakai, H.; Zakharov, L. N.; Rheingold, A. L.; Meyer, K. *Science* **2004**, *305*, 1757–1759.
(5) (a) Gagliardi, L.; Roos, B. O. *Nature* **2005**, *433*, 848–851. (b) Straka, M.; Pyykkö, P. *J. Am. Chem. Soc.* **2005**, *127*, 13090–13091.

group 13 diyls Cp*E (E = Al, Ga) provide useful synthons for preparing new *f*-element metal−metal bonded species.[8] In this manner, and using starting materials similar to those developed by Andersen and co-workers for studying M−CO complexes (M = Ca, Eu, Yb, U),[9] Roesky and co-workers recently discovered a series of 4*f*-group 13 metal bonds: $Cp^*_2Ln-AlCp^*$ (Ln = Eu, Yb), $Cp^*_2Eu(GaCp^*)_2$, and $Cp^*_2Yb(THF)-GaCp^*$.[10] Along similar lines we recently reported the first example of unsupported metal−metal bonding between 5*f* and group 13 elements: $(CpSiMe_3)_3U-AlCp^*$.[11]

Marks and co-workers' actinide−transition metal complexes were prepared alternatively, through metathesis.[3] More recently, the complex $[(tren\text{-}SiMe_3)(THF)U-Ga(NArCH)_2]$ (tren-$SiMe_3$ = $N(CH_2CH_2NSiMe_3)$, Ar = 2,6-$Pr^i_2C_6H_3$) was prepared from an anionic Ga N-heterocyclic carbene (NHC) analogue.[12] Remarkably, DFT calculations suggest the strongly electrostatic U−Ga bond also exhibits π-donation from the Ga-heterocycle to an empty $5f_{z^2y}$ orbital on U. Further illustrating the utility of this synthetic strategy, an unsupported U−Re bond was also reported.[13]

In the simplest sense, Cp*E are typical σ-donors[14] and are also formally isolobal with carbon monoxide and singlet carbenes.[15] The HOMO of Cp*E consists predominantly of a large lobe on E, directed away from the Cp* ligand, and the two orthogonal, degenerate LUMOs are π-antibonding with respect to the Cp*−E bond. Back-bonding of π-electrons from electron-rich metals to Cp*M could, in theory, exist in the otherwise purely dative interactions; however this has not been observed with transition metals.[15]

While it is now well-known that some *f*-elements can engage in covalent bonding, elucidating the degree of covalency in otherwise predominately electrostatic or dative bonds is both a historical and current topic of significant synthetic and theoretical interest.[16] The suggestion that better 4*f*/5*f* element separations are achieved with π-accepting ligands underscores the importance of research in this area.[17] Comparisons of lanthanide and actinide reactivity[18] are also of fundamental interest regarding differences in the radial extension of 4*f* and 5*f* valence orbitals.[19] Only a handful of examples are known in which a pair of isoelectronic and isostructural 4*f*/5*f* compounds have been reported, including $((SiMe_3)_2N)_3M$,[20] Cp^*_3M,[21] $[(Cp(SiMe_3)_2]_3M$,[18a,22] and Cp_3M-THF[23] (M = Nd, U). This lack of data has convoluted the analysis of reactivity patterns due to the metal from differences in the ligand set.

Herein, we compare the reactivity of an isoelectronic and isostructural system of 4*f* and 5*f* complexes, $(CpSiMe_3)_3U$ and $(CpSiMe_3)_3Nd$, in the context of their complexes with Cp*Ga and Cp*Al. The U complexes were isolated on gram scales and characterized by standard techniques, while the Nd complexes were observed spectroscopically. Each complex features a new unsupported metal−metal bond, the stabilities of which were evaluated by variable-temperature ^{1}H NMR and DFT calculations. Excellent 5*f*/4*f* discrimination is demonstrated based on small-scale competition experiments. An in-depth experimental and theoretical study of the metal−ligand bonding modes is also presented.

Results and Discussion

Synthesis and Structural Characterization of Uranium Complexes. In a recent communication, we described the synthesis and characterization of $(CpSiMe_3)_3U-AlCp^*$ (**1**).[11] Two crystallographically inequivalent molecules comprise the asymmetric unit in crystals of **1**, with U−Al bond lengths (U(1A)−Al(1A), 3.117(3) Å; U(1B)−Al(1B), 3.124(4) Å) which are both similar to the sum of U and Al covalent radii[24] (U + Al = 3.17(13) Å).

Building upon this discovery, the combination of $(CpSiMe_3)_3U$ and Cp*Ga in a minimal amount of pentane resulted in a nearly instantaneous reaction which was accompanied by a darkening of the green solution. Whereas **1** is red/brown in solution, solutions of **2** retained more of the original green color exhibited by $(CpSiMe_3)_3U$. Crystallization at −80 °C produced very dark green, X-ray quality blocks of $(CpSiMe_3)_3U-GaCp^*$ (**2**) in 90% yield (eq 1). The presence of bridging hydrides was ruled out according to a previously outlined series of experiments.[11] The structural features of **1** and **2**, as well as their optical spectra and magnetic properties

(6) (a) Arnold, P. L.; Jones, N. A.; Carmichael, C. D. *Inorg. Chem.* **2008**, *47*, 8577–8579. (b) Graves, C. R.; Schelter, E. J.; Cantat, T.; Scott, B. L.; Kiplinger, J. L. *Organometallics* **2008**, *27*, 5371–5378.
(7) For a comprehensive review of *f*-element metal−metal bonding, see: Liddle, S. T.; Mills, D. P. *Dalton Trans.* **2009**, 5592–5605.
(8) Roesky, P. W. *Dalton Trans.* **2009**, 1887–1893.
(9) (a) Brennan, J. G.; Andersen, R. A.; Robbins, J. L. *J. Am. Chem. Soc.* **1986**, *108*, 335–336. (b) Selg, P.; Brintzinger, H. H.; Andersen, R. A.; Horváth, I. T. *Angew. Chem., Int. Ed. Engl.* **1995**, *34*, 791–793. (c) Schultz, M.; Burns, C. J.; Schwartz, D. J.; Andersen, R. A. *Organometallics* **2001**, *20*, 5690–5699.
(10) (a) Gamer, M. T.; Roesky, P. W.; Konchenko, S. N.; Nava, P.; Ahlrichs, R. *Angew. Chem., Int. Ed.* **2006**, *45*, 4447–4451. Wiecko, M.; Roesky, P. W. *Organometallics* **2007**, *26*, 4846–4848.
(11) Minasian, S. G.; Krinsky, J. L.; Williams, V. A.; Arnold, J. *J. Am. Chem. Soc.* **2008**, *130*, 11262–11263.
(12) Liddle, S. T.; McMaster, J.; Mills, D. P.; Blake, A. J.; Jones, C.; Woodul, W. D. *Angew. Chem., Int. Ed.* **2008**, *48*, 1077–1080.
(13) Gardner, B. M.; McMaster, J.; Lewis, W.; Liddle, S. T. *Chem. Commun.* **2009**, 2851–2853.
(14) Cadenbach, T.; Gemel, C.; Schmid, R.; Halbherr, M.; Ysenko, K.; Cokoja, M.; Fischer, R. D. *Angew. Chem., Int. Ed.* **2009**, *48*, 3872–3876.
(15) Gemel, C.; Steinke, T.; Cokoja, M.; Kempter, A.; Fischer, R. A. *Eur. J. Inorg. Chem.* **2004**, 4161–4176.
(16) (a) Raymond, K. N.; Eigenbrot, C. W. *Acc. Chem. Res.* **1980**, *13*, 276–283. (b) Kozimor, S. A.; Yang, P.; Batista, E. R.; Boland, K. S.; Burns, C. J.; Christensen, C. N.; Clark, D. L.; Conradson, S. D.; Hay, P. J.; Lezama, J. S.; Martin, R. L.; Schwarz, D. E.; Wilkerson, M. P.; Wolfsberg, L. E. *Inorg. Chem.* **2008**, *47*, 5365–5371.
(17) (a) Wietzke, R.; Mazzanti, M.; Latour, J. M.; Pecaut, J.; Cordier, P. Y.; Madic, C. *Inorg. Chem.* **1998**, *37*, 6690–6697. (b) Mazzanti, M.; Wietzke, R. L.; Pecaut, J.; Latour, J. M.; Maldivi, P.; Remy, M. *Inorg. Chem.* **2002**, *41*, 2389–2399. (c) Mehdoui, T.; Berthet, J.-C.; Thuéry, P.; Ephritikhine, M. *Dalton Trans.* **2004**, 579–590. (d) Mehdoui, T.; Berthet, J.-C.; Thuéry, P.; Ephritikhine, M. *Chem. Commun.* **2005**, 2860–2862. (e) Maron, L.; Bourissou, D. *Organometallics* **2009**, *28*, 3686–3690.
(18) (a) Conejo, M. D.; Parry, J. S.; Carmona, E.; Schultz, M.; Brennann, J. G.; Beshouri, S. M.; Andersen, R. A.; Rogers, R. D.; Coles, S.; Hursthouse, M. *Chem.−Eur. J.* **1999**, *5*, 3000–3009. (b) Evans, W. J.; Kozimor, S. A.; Nyce, G. W.; Ziller, J. W. *J. Am. Chem. Soc.* **2003**, *125*, 13831–13835.
(19) (a) Crosswhite, H. M.; Crosswhite, H.; Carnall, W. T.; Paszek, A. P. *J. Chem. Phys.* **1980**, *72*, 5103–5117. (b) Strittmatter, R. J.; Bursten, B. E. *J. Am. Chem. Soc.* **1991**, *113*, 552–559.
(20) (a) Andersen, R. A.; Templeton, D. H.; Zalkin, A. *Inorg. Chem.* **1978**, *17*, 2317–2319. (b) Stewart, J. L.; Andersen, R. A. *Polyhedron* **1998**, *17*, 953–958.
(21) (a) Evans, W. J.; Seibel, C. A.; Ziller, J. W. *J. Am. Chem. Soc.* **1998**, *120*, 6745–6752. (b) Evans, W. J.; Nyce, G. W.; Forrestal, K. J.; Ziller, J. W. *Organometallics* **2002**, *21*, 1050–1055.
(22) Xie, Z. W.; Chui, K. L.; Liu, Z. X.; Xue, F.; Zhang, Z. Y.; Mak, T. C. W.; Sun, J. *J. Organomet. Chem.* **1997**, *549*, 239–244.
(23) (a) Wasserman, H. J.; Zozulin, A. J.; Moody, D. C.; Ryan, R. R.; Salazar, K. V. *J. Organomet. Chem.* **1983**, *254*, 305–311. (b) Benetollo, F.; Bombieri, G.; Castellani, C. B.; Jahn, W.; Fischer, R. D. *Inorg. Chim. Acta* **1984**, *95*, L7–L10.
(24) Cordero, B.; Gómez, V.; Platero-Prats, A. E.; Revés, M.; Echeverría, J.; Cremades, E.; Barragán, F.; Alvarez, S. *Dalton Trans.* **2008**, 2832–2838.

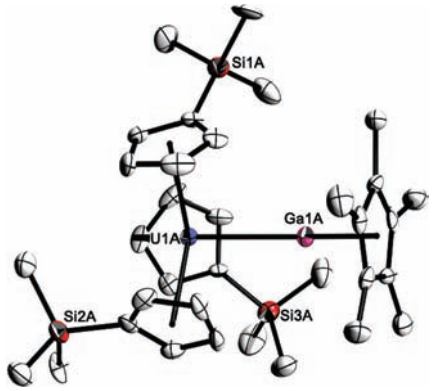

Figure 1. Molecular structure of **2A**. Thermal ellipsoids are drawn at the 50% probability level. Hydrogen atoms have been removed for clarity. Selected bond lengths (Å) and angles (deg): U(1A)−Ga(1A), 3.0648(12); Ga(1A)−Ct(4A), 1.976(4); U(1A)−Ct(1A), 2.531(13); U(1A)−Ct(2A), 2.523(12); U(1A)−Ct(3A), 2.529(12); U(1A)−Ga(1A)−Ct(4A), 161.3(4); Ct(1A)−U(1A)−Ct(2A), 115.1(5); Ct(1A)−U(1A)−Ct(3A), 119.9(4); Ct(2A)−U(1A)−Ct(3A), 119.9(5).

(see below), are consistent with U(III)/Al(I) and U(III)/Ga(I) formal oxidation state assignments.

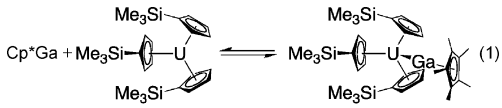

2

Crystalline **2** is isostructural with **1** (Figure 1); two inequivalent molecules **2A** and **2B** are also present in the asymmetric unit of the crystal lattice. The coordination geometry is slightly distorted from an ideal trigonal pyramidal geometry, with the sum of the Ct−U(1A)−Ct (Ct = Cp centroid) angles totaling 354.96°. The U(1A)−Ga(1A)−Ct(4A) angle (161.29°) is distorted from linearity. As was observed with **1**, the Ga(1A)−Ct(4A) distance (1.976 Å) is slightly shorter than that observed in that of the parent organyl, in this case hexameric $(Cp^*Ga)_6$ (2.081 Å).[25]

The uranium−gallium bond lengths (U(1A)−Ga(1A), 3.0648(12) Å; U(2A)−Ga(2B), 3.0800(13) Å) are shorter than the sums of their covalent radii (U + Ga = 3.18(10) Å) and are *ca.* 0.05 Å shorter than the U−Al bonds in **1**, though Al and Ga have similar covalent radii (Al = 1.21(4) Å, Ga = 1.22(3) Å). These U(III)−Ga(I) bonds are also shorter than those observed in the U−Ga complex prepared by Liddle and Jones (again, two molecules are present: U(1)−Ga(1), 3.2115(8) Å; U(2)−Ga(2), 3.2983(9) Å).[12] These bond distances, especially considering the difference between those of the two identical molecules in the unit cell, are no doubt influenced by crystal packing forces and may not correlate with bond strength (see below).

Synthesis and Structural Characterization of $(CpSiMe_3)_3Nd$. The synthesis of $(CpSiMe_3)_3Nd$[26] proceeded by conventional methods involving treatment of $NdCl_3$ with $(CpSiMe_3)K$ in refluxing toluene. The product was isolated in 67% yield as yellow-green needles following crystallization from toluene and was characterized by standard analytical means. The molecule is isostructural with $(CpSiMe_3)_3Ce$ and

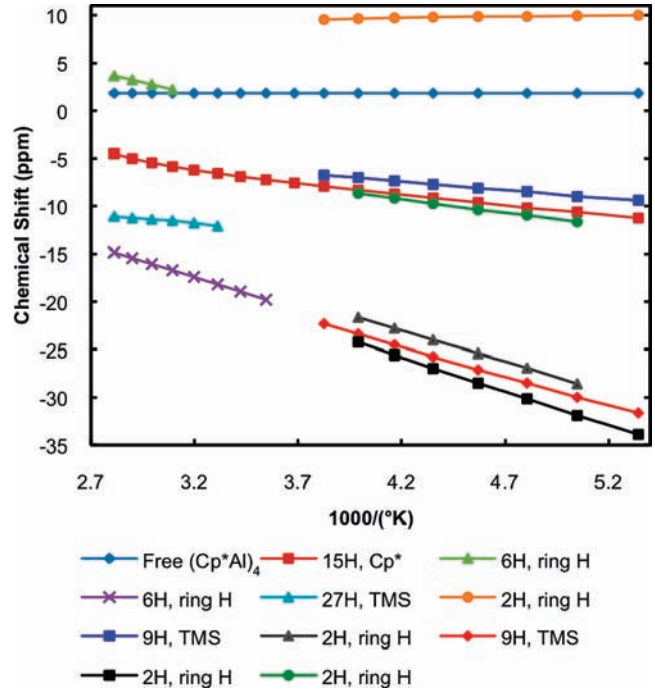

Figure 2. Variable temperature ^{1}H NMR behavior of $(CpSiMe_3)_3UAlCp^*$ (**1**), δ vs $1/T$.

$(CpSiMe_3)_3U$ (see Supporting Information, Figure S10),[27] with an average Nd−Ct distance (*ca.* 2.49 Å) that is very close to that of $(CpSiMe_3)_3U$ (*ca.* 2.51 Å).

NMR Spectroscopy of Aluminum Complexes. The tetramer $(Cp^*Al)_4$ exists in equilibrium with its monomer Cp*Al,[28] with a ΔH for tetramerization of 9(1) kcal mol^{-1} per monomer as shown by variable-temperature ^{27}Al NMR experiments (eq 2).[29] Accordingly, the equilibria represented by eq 3 were examined by dynamic ^{1}H NMR spectroscopy.

$$^1/_4(Cp^*Al)_4 \rightleftharpoons Cp^*Al \quad (\Delta H = 9(1)\ \text{kcal mol}^{-1}) \qquad (2)$$

$$^1/_4(Cp^*Al)_4 + (CpSiMe_3)_3M \rightleftharpoons (CpSiMe_3)_3M(AlCp^*) \qquad (3)$$
$$M = U\ (\mathbf{1}),\ M = Nd\ (\mathbf{3})$$

We have revised our preliminary assignments for the ^{1}H NMR spectra of **1** that were flawed due to unusual dynamic and paramagnetic behavior which obscured peaks between −90 and +50 °C. A plot of chemical shift vs $1/T$ is presented in Figure 2; these data are available in tabular form with line widths in the Supporting Information, as are tables of ^{1}H NMR data for the other relevant compounds.

At 19 °C, one very broad signal was observed at δ −11.95 (27 H, $\nu_{1/2}$ = 2300 Hz), corresponding to the three $SiMe_3$ groups, as was another sharper peak at δ −18.95 (6 H, $\nu_{1/2}$ = 79 Hz) corresponding to one set of Cp ring protons. On raising the temperature to 50 °C, these signals sharpened and an additional

(25) Loos, D.; Baum, E.; Ecker, A.; Schnöckel, H.; Downs, A. J. *Angew. Chem., Int. Ed. Engl.* **1997**, *36*, 860–863.
(26) No preparation has been reported, although $(CpSiMe_3)_3Nd$ is known. Jank, S.; Reddmann, H.; Amberger, H. D.; Apostolidis, C. *J. Organomet. Chem.* **2004**, *689*, 3143–3157.
(27) (a) Zalkin, A.; Brennan, J. G.; Andersen, R. A. *Acta Crystallogr., Sect. C* **1988**, *44*, 2104–2106. (b) Stults, S. D.; Andersen, R. A.; Zalkin, A. *Organometallics* **1990**, *9*, 115–122.
(28) Dohmeier, C.; Loos, D.; Schnöckel, H. *Angew. Chem., Int. Ed. Engl.* **1996**, *35*, 129–149.
(29) (a) Dohmeier, C.; Robl, C.; Tacke, M.; Schnöckel, H. *Angew. Chem., Int. Ed.* **1991**, *30*, 564–565. (b) Gauss, J.; Schneider, U.; Ahlrichs, R.; Dohmeier, C.; Schnöckel, H. *J. Am. Chem. Soc.* **1993**, *115*, 2402–2408.

broad peak appeared at δ 2.22 (6 H, $\nu_{1/2} = 247$ Hz), which was assigned to the other set of ring protons.

When the temperature was lowered, all the $CpSiMe_3$ ligand signals continued to broaden and became almost completely indiscernible from the baseline at 0 °C. Between −12 and −75 °C, a new set of signals were visible corresponding to two $CpSiMe_3$ ligands. The third set of $CpSiMe_3$ signals were not discernible in this temperature range, and based on peak intensities, it is unlikely that they are coincident with other resonances. In $(CpSiMe_3)_3U$ all three ligands display equivalent signals; the separation of the $CpSiMe_3$ ligand peaks indicates that the Cp*Al ligand does not exhibit fast-exchange behavior in this temperature range. As the temperature was lowered below −75 °C, these signals continued to broaden into the baseline. At all measured temperatures two signals were observed corresponding to protons in $(Cp^*Al)_4$ and the Cp* protons in **1**, as expected according to eq 3.

Because Cp*Al undergoes an exothermic tetramerization, we did not expect to observe the formation of the presumably weakly bound $(CpSiMe_3)_3Nd-AlCp^*$ (**3**). Indeed, no color change was observed upon adding $(Cp^*Al)_4$ to solutions of $(CpSiMe_3)_3Nd$, and a ^1H NOESY NMR experiment did not provide evidence of an interaction. All attempts to precipitate or crystallize **3** were unsuccessful. In spite of this, a number of observations regarding the NMR spectra of $(CpSiMe_3)_3Nd$ in the presence of $(Cp^*Al)_4$ suggest that **3** exists in small amounts, particularly at elevated temperature.

As reported in the literature,[28,29] the ^{27}Al NMR spectrum of $(Cp^*Al)_4$ (δ −80 ppm) in d_8-toluene develops a second peak at δ −150 ppm above *ca.* 50 °C which is assigned to monomeric Cp*Al. Under the same conditions, but including 1 mol equiv of $(CpSiMe_3)_3Nd$, no peak corresponding to the monomer was observed. Additionally, at 83 °C the chemical shifts of the $CpSiMe_3$ ligand protons were shifted from those of pure $(CpSiMe_3)_3Nd$ by *ca.* 1.0 to 2.5 ppm. Most importantly, the spectral line widths for samples of pure $(CpSiMe_3)_3Nd$ with and without added $(Cp^*Al)_4$ were dramatically different. For example, between 40 and 83 °C, the relatively broad $SiMe_3$ resonance observed for pure $(CpSiMe_3)_3Nd$ ($\nu_{1/2}$ = 47 to 76 Hz) narrowed on addition of $(Cp^*Al)_4$ ($\nu_{1/2}$ = 8.1 to 14 Hz). After careful scrutiny of the ^1H NMR baseline we discerned a weak signal which we assign to the Cp* protons in **3**. Upon cooling to room temperature the spectra of $(CpSiMe_3)_3Nd$ with and without $(Cp^*Al)_4$ became nearly indistinguishable with regard to peak positions and line widths. Tables of ^1H NMR data and plots comparing the $\nu_{1/2}$ for both systems are available in the Supporting Information.

NMR Spectroscopy of Gallium Complexes. Unlike $(Cp^*Al)_4$, Cp*Ga is monomeric in solution, and accordingly the equilibria represented by eq 4 were examined by ^1H NMR spectroscopy. The variable-temperature ^1H NMR behavior of **2** indicated it is in rapid equilibrium with starting materials over a broad temperature range. At 72 °C the signals were relatively sharp for the downfield and upfield ring protons ($\nu_{1/2}$ = 18 and 22 Hz, respectively) and $SiMe_3$ protons ($\nu_{1/2}$ = 8.1 Hz). As the temperature was lowered these signals broadened, and below −56 °C (−88 °C for the upfield ring protons) they became indiscernible from the baseline. An additional broad peak which appeared below −78 °C could not be assigned. At all measured temperatures, a single sharp paramagnetically shifted signal was observed for the Cp* protons in both **2** and free Cp*Ga; the chemical shift is a weighted average depending on the concentration of each species (see below).

$$Cp^*Ga + (CpSiMe_3)_3M \rightleftharpoons \underset{M = U\ (\mathbf{2}),\ M = Nd\ (\mathbf{4})}{(CpSiMe_3)_3M(GaCp^*)} \quad (4)$$

Because Cp*Ga does not competitively form aggregates,[28] formation of $(CpSiMe_3)_3Nd-GaCp^*$ (**4**) was expected to be much more facile than formation of **3** regardless of the Nd−Ga bond strength. Still, addition of *ca.* 1 equiv of Cp*Ga to a solution of $(CpSiMe_3)_3Nd$ did not result in a color change, and all attempts to isolate crystalline **4** were unsuccessful. However, two primary differences were noted in the ^1H NMR spectra of $(CpSiMe_3)_3Nd$ with and without Cp*Ga. When combined at −33 °C, the resonance for the Cp* protons was paramagnetically shifted upfield by >1 ppm from that of free Cp*Ga (1.92 ppm),[30] and the $CpSiMe_3$ peaks were shifted by 2−3 ppm from those in pure $(CpSiMe_3)_3Nd$. Also at −33 °C, the $CpSiMe_3$ peak line widths for the $SiMe_3$, downfield and upfield ring protons narrowed substantially in the presence of Cp*Ga (70.4, 68, and 20.0 Hz, respectively) in comparison with those of pure $(CpSiMe_3)_3Nd$ ($\nu_{1/2}$ = 120, 91, and 47 Hz, respectively). (For a table and plots of chemical shift and line-width data, see the Supporting Information.)

Determination of Thermodynamic Parameters by NMR Titration. For systems undergoing fast ligand exchange, NMR titration is a useful method that allows very precise measurement of thermodynamic data because it is based on chemical shift measurements, not on peak intensitites.[31] Ephritikhine and co-workers have reported extensively on the thermodynamics of tris(cyclopentadienyl) uranium complexes in the presence of substituted pyridines under fast-exchange conditions.[17c] Because Cp*Al aggregates and is prone to crystallization from solution, thermodynamic measurements could not be made for **1** or **3**. However, the excellent solubility properties of Cp*Ga render **2** and **4** ideal for thermodynamic measurements on analogous *4f*/*5f* compounds.

For 0.05−0.10 M solutions of $(CpSiMe_3)_3M$ (M = Nd, U) in d_8-toluene with n equiv of Cp*Ga, the three signals corresponding to the $CpSiMe_3$ ligands trend away from those of free $(CpSiMe_3)_3M$ and toward limit positions corresponding to complete formation of product **2** or **4**. The observed chemical shifts for the $CpSiMe_3$ ligands (δ_{obs}) are weighted averages of those of $(CpSiMe_3)_3M$ (δ_M) and product (δ_{MGa}) and depend on the molar fraction of product (x_{MGa}) present in solution ($x_{MGa} = (\delta_{obs} - \delta_M)/(\delta_{MGa} - \delta_M)$), which is proportional to the equilibrium constant (K_{MGa}).[17c] Successful implementation of this method requires determination of the limit spectrum (δ_{MGa}). For **2**, this was achieved with n = 9 equiv of Cp*Ga between 22 and 72 °C. However, the limit spectrum for **4** (δ_{NdGa}) could not be determined in the same temperature range, even with n > 100. Instead, determination of the limit spectrum (δ_{NdGa}) was achieved with n = 10 between −33 and 19 °C.

Examination of the equilibrium constants, obtained at room temperature, for **2** (K_{UGa} = 21.4(2)) and **4** (K_{NdGa} = 2.0(1)), suggests that both complexes are considerably less stable than the pyridine complex of $(CpSiMe_3)_3U$ ($K_{UL} = 3(1) \times 10^4$) but of similar stability to the pyridine complex of $(CpCMe_3)_3U$ (K_{UL} = 45(3)).[17c] Although both interactions are weak, **2** is more stable than **4** by an order of magnitude, suggesting that U is a much better acceptor than Nd in this system.

(30) Jutzi, P.; Schebaum, L. O. *J. Organomet. Chem.* **2002**, *654*, 176–179.
(31) Perrin, C. L.; Dong, Y. M. *J. Am. Chem. Soc.* **2007**, *129*, 4490–4497.

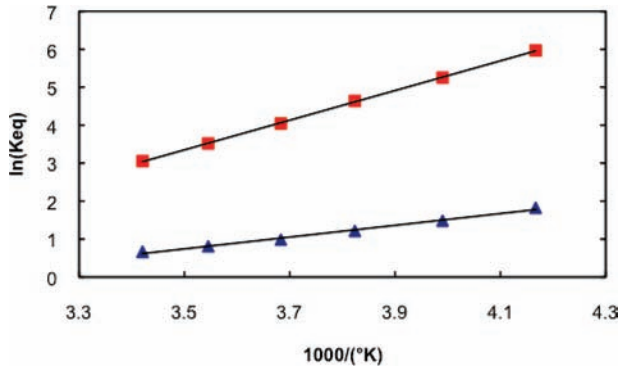

Figure 3. Representative van't Hoff plot of $\ln(K_{eq})$ vs $1/T$ for the formation of $(CpSiMe_3)_3MGaCp^*$ (**2**, M = U, red squares; **4**, M = Nd, blue triangles).

Table 1. U(III)/Nd(III) Competition Reactions Including Molar Fractions (x), Separation Factors ($S_{U/Nd}$),[a] and Speciation Percentages[b] of **2** and **4**

T (°C)	x_{UGa}	x_{NdGa}	$S_{U/Nd}$	% **2**	% **4**
−33	0.780(4)	0.0329(1)	23.2(5)	95.9(1)%	4.1(1)%
−23	0.701(6)	0.0340(1)	20.4(3)	95.3(1)%	4.7(1)%
−12	0.612(7)	0.0324(5)	19.0(6)	95.0(2)%	5.0(2)%
−1.6	0.522(7)	0.0318(6)	16.3(7)	94.2(2)%	5.8(2)%
8.9	0.434(7)	0.0268(1)	15.4(3)	93.9(1)%	6.1(1)%
19	0.353(5)	0.0233(1)	13.9(2)	93.3(1)%	6.7(1)%

[a] $S_{U/Nd} = x_{UGa}/x_{NdGa}$. [b] Percentage of the total formation of **2** or **4**, calculated by setting $x_{UGa} + x_{NdGa} = 1$, such that speciation % $= x_{MGa}/(x_{UGa} + x_{NdGa})$.

A representative van't Hoff plot of $\ln(K_{MGa})$ *vs* $1/T$ for **2** and **4** is shown in Figure 3. Measurements and standard deviations were obtained from multiple, independently prepared samples and various concentrations of Cp*Ga (see the Supporting Information for all data). For **2**, the thermodynamic parameters ΔH_{UGa} (−5.8(2) kcal mol^{-1}) and ΔS_{UGa} (−13.4(6) cal mol^{-1} K^{-1}) are approximately 3 times smaller than those for $(CpSiMe_3)_3U-pyr$ (pyr = pyridine, $\Delta H_{UL} = -18(2)$ kcal mol^{-1}, $\Delta S_{UL} = -39(4)$ cal mol^{-1} K^{-1}), and somewhat less than those observed for $(CpSiMe_3)_3U-THF$ ($\Delta H_{UL} = -9.8(2)$ kcal mol^{-1}) and $(CpSiMe_3)_3U-CO$ ($\Delta H_{UL} = 10.3(2)$ kcal mol^{-1}).[17c,32] For **4**, the thermodynamic parameters ΔH_{NdGa} (−3.0(2) kcal mol^{-1}) and ΔS_{NdGa} (−9.1(7) cal mol^{-1} K^{-1}) are approximately five times smaller than those for the cerium complex $(CpSiMe_3)_3Ce-pyr$ ($\Delta H_{CeL} = -15(2)$ kcal mol^{-1}, $\Delta S_{CeL} = -35(3)$ cal mol^{-1} K^{-1}).

Competition Reactions: U vs Nd. Competition reactions of $(CpSiMe_3)_3Nd$ and $(CpSiMe_3)_3U$ with Cp*Ga were monitored by ^{1}H NMR spectroscopy according to the method outlined by Ephritikhine and co-workers.[17c] The experiments were performed on multiple independent samples, and results were reproducible. Both products **2** and **4** were formed upon addition of 1 equiv of Cp*Ga (relative to U or Nd) to a 1:1 mixture of $(CpSiMe_3)_3Nd$ and $(CpSiMe_3)_3U$ in d_8-toluene. The molar fractions of each product (x_{MGa}), separation factors ($S_{U/Nd}$), and speciation percentages (summed to unity) are listed in Table 1. Relatively large molar fractions of product are observed, especially at −33 °C, and a common trend toward enhanced selectivity at lower temperatures is also observed in these systems. Excellent 5*f*/4*f* selectivity was observed for Cp*Ga, with $S_{U/Nd} = 13.9(2)$ and a 93.3(1):6.7(1) product ratio near room temperature and $S_{U/Nd} = 23.2(5)$ with a 95.9(1):4.1(1) product ratio at −33 °C. By comparison, the separation factor for dimethylpyrazine is 3.3(2) for $(CpSiMe_3)_3M$ (M = Ce, U) at 23 °C,[17c] and up to 90:10 product ratios were observed at −60 °C for $(CpCMe_3)_3M$ (M = Ce, U) with NHC ligands.[17d]

As was explained regarding thermodynamic measurements, because monomeric Cp*Al readily tetramerizes to form insoluble $(Cp^*Al)_4$, and limit behavior could not be observed for **3**, a separation factor $S_{U/Nd}$ for Cp*Al could not be determined. However, a sample containing 0.25 mol equivalent of tetrameric $(Cp^*Al)_4$ (relative to U or Nd) and a 1:1 mixture of $(CpSiMe_3)_3Nd$ and $(CpSiMe_3)_3U$ in d_8-toluene at 21 °C contained, on the basis of ^{1}H NMR peak intensities, only trace **3** and levels of **1** that were not detectably reduced from samples of the pure material. This excellent U(III)/Nd(III) selectivity may be expected if formation of **1** is favorable, and formation of **3** is unfavorable, relative to tetramerization of Cp*Al (9(1) kcal mol^{-1}). Though reproducible these measurements are at the limit of error for this method, and we are currently exploring alternative methods to evaluate 4*f*/5*f* selectivity in this system.

Competition Reactions: Al vs Ga. A series of exploratory competition experiments were performed to perturb the equilibria depicted in eq 5 and evaluate the donor ability of Cp*Al and Cp*Ga relative to other simple monodentate ligands.

$$\underset{\text{E = Al (1), E = Ga (2)}}{(CpSiMe_3)U(ECp^*)} + L \rightleftharpoons \underset{\text{(E = Al, } x = 1/4\text{; E = Ga, } x = 1)}{(CpSiMe_3)_3U(L) + (Cp^*E)_x} \quad (5)$$

Andersen and co-workers have previously used a similar method to quantitatively determine the comparative efficacy of pyridine and PMe_3 as ligands for $(C_5H_4R)_3U$ (R = H, Me, $SiMe_3$);[33] only qualitative comparisons are made here. A 1 molar equiv amount (*ca.* 4 equiv in the case of CO) of ligand (L) was added to a solution of **1** or **2** in C_6D_6, and a ^{1}H NMR spectrum was collected. The resulting spectra along with reference data for **1**, **2**, $(Cp^*Al)_4$, and Cp*Ga are summarized in Table 2.

We interpret these results as follows: when L = Et_2O, the peak positions and line widths of **1** and **2** were not significantly altered and no new peaks were observed, and thus, Et_2O does not displace Cp*E from the U(III) atom. When L = THF, a paramagnetically shifted peak attributable to the Cp* protons was observed, indicating that some **1** or **2** remained in solution. We observed almost complete formation of the new products in the presence of pyridine or PMe_3 with **1** or **2** at room temperature; however **1** is observed above 50 °C in the presence of PMe_3. Finally, addition of excess CO completely displaced Cp*Al from **1**, resulting in the formation of $(Cp^*Al)_4$ crystals and $(CpSiMe_3)_3U-CO$, as assigned by ^{1}H NMR and IR spectroscopy.[9a] Interestingly, though an analogous reaction of CO with **2** also resulted in formation of $(CpSiMe_3)_3U-CO$, the Cp* peak is paramagnetically shifted indicating that some **2** persists in the presence of CO. The difference in reactivity of **1** and **2** toward CO likely stems from the fact that Cp*Ga remains a monomer in solution, while free Cp*Al forms a thermodynamically favorable tetramer.

For all other choices of L, irreversible reactions were observed by ^{1}H NMR spectroscopy. Addition of excess CO_2 to solutions of **1** or **2** in C_6D_6 resulted in formation of $[(CpSiMe_3)_3U]_2(\mu\text{-}O)$;[34] analogous reactions with CS_2 also produced the anticipated $[(CpSiMe_3)_3U]_2(\mu\text{-}CS_2)$ product.[35] Reactions with excess

(32) Schock, L. E.; Seyam, A. M.; Sabat, M.; Marks, T. J. *Polyhedron* **1988**, *7*, 1517–1529.

(33) Brennan, J. G.; Stults, S. D.; Andersen, R. A.; Zalkin, A. *Inorg. Chim. Acta* **1987**, *139*, 201–202.

Table 2. Results of ^{1}H NMR Scale Competition Reactions between **1** or **2** and Small Molecules (L)

starting material	L	equiv of L	*T* (°C)	δ ($\nu_{1/2}$)				
				free $(Cp^*Al)_4$	bound Cp*E	6H, ring CH	6H, ring CH	27H, $SiMe_3$
1	−	−	19	1.84 (1.4)	−6.89 (4.6)	−	−18.95 (79)	−11.95 (2300)
1	−	−	50	1.84 (2.0)	−5.84 (6.4)	2.22 (250)	−16.70 (26)	−11.53 (180)
1	Et_2O	1	22	1.89 (1.5)	−6.92 (5.0)	−	−18.45 (65)	−12.22 (1500)
1	THF	1	50	1.90 (1.9)	−5.00 (14)	−0.83 (118)	−16.19 (200)	−9.76 (65)
1	pyridine	1	22	1.90 (2.0)	−	−3.24 (190)	−19.72 (69)	−5.15 (290)
1	pyridine	1	50	1.90 (1.9)	−	−1.95 (67)	−17.21 (23)	−5.45 (81)
1	PMe_3	1	22	1.90 (1.3)	−	−8.97 (460)	−13.36 (210)	−5.64 (240)
1	PMe_3	1	50	1.90 (2.5)	−3.25 (51)	−6.57 (170)	−12.44 (52)	−5.72 (73)
1	CO	*ca.*4	22	1.89 (1.1)	−	−2.20 (150)	−16.75 (29)	−6.59 (110)
−	$(Cp^*Al)_4$	−	22	1.91 (2.04)	−	−	−	−
2	−	−	22	N/A	−1.12 (9.0)	4.49 (50)	−19.08 (24)	−14.86 (27)
2	Et_2O	1	22	N/A	−1.14 (8.5)	6.01 (42)	−19.30 (27)	−16.24 (24)
2	THF	1	22	N/A	1.15 (5.3)	−1.90 (83)	−17.92 (31)	−8.17 (61)
2	CO	*ca.*4	22	N/A	1.29 (1.9)	−2.385 (85)	−16.62 (26)	−6.06 (70)
2	PMe_3	1	22	N/A	1.91 (2.1)	−9.92 (28)	−12.88 (24)	−4.99 (5.0)
2	pyridine	1	22	N/A	1.92 (2.1)	−3.72 (20)	−19.99 (29)	−4.38 (5.4)
−	Cp*Ga	−	22	N/A	1.93 (0.89)	−	−	−

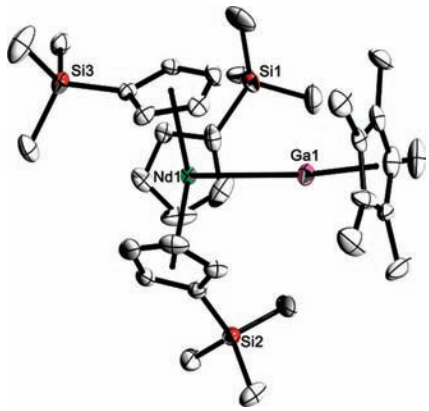

Figure 4. Molecular structure of **3**, with a molecule of $[(CpSiMe_3)_2Nd(\mu\text{-}OH)]_2$, hydrogen atoms, and disorder around both the C_5Me_5 ring and Si(1b) omitted for clarity. Thermal ellipsoids are drawn at the 50% probability level. Selected bond lengths (Å): Nd(1)−Ga(1), 3.1526(6); Ga(1)−Ct(4), 1.9377(5); Nd(1)−Ct(1), 2.5154(3); Nd(1)−Ct(2), 2.5270(2); Nd(1)−Ct(3), 2.5116(2).

$B(C_6F_5)_3$ resulted in the donor−acceptor complexes $Cp^*E{-}B(C_6F_5)_3$ and a new unidentified paramagnetic product.[36]

Attempts To Isolate Neodymium Complexes. As stated above, exhaustive efforts to isolate crystalline **3** or **4** from concentrated and cooled solutions were unsuccessful. In one instance, however, a sample of $(CpSiMe_3)_3Nd$ dissolved in neat Cp*Ga afforded a few milligrams of small, colorless blocks. An X-ray crystal structure revealed a crystal lattice containing two species, $[(CpSiMe_3)_2Nd(\mu\text{-}OH)]_2$ and $(CpSiMe_3)_3NdGaCp^*$ (**4**) (Figure 4). To the best of our knowledge, the preparation of $[(CpSiMe_3)_2Nd(\mu\text{-}OH)]_2$ has not been reported, although the closely related species $[(CpCMe_3)_2Nd(\mu\text{-}OH)]_2$ has been described.[26] Attempts to reproduce this result by more rational means failed, though a ^{1}H NMR experiment revealed that adding 0.5 equiv of H_2O to a solution of 1:1 $(CpSiMe_3)_3Nd$ and Cp*Ga formed a mixture containing 1 equiv of protonated $CpSiMe_3$, as well as unreacted $(CpSiMe_3)_3Nd$ and Cp*Ga. Peaks attributable to formation of $[(CpSiMe_3)_2Nd(\mu\text{-}OH)]_2$ were not observed, although signals from this species may be obscured due to paramagnetism (we note that NMR data for $[(CpCMe_3)_2Nd(\mu\text{-}OH)]_2$ were not reported).

The serendipitous cocrystallization of **4** along with the hydroxide (which presumably acts as a crystallization agent in this instance), while not attractive synthetically, nonetheless provides useful metrical information on a weakly bound complex which is otherwise unattainable. These data show that **4** is isostructural with **1** and **2** and provide structural evidence of an unsupported Nd−Ga bond. The neodymium atom approaches ideal trigonal pyramidal geometry, with the sum of the Ct−Nd(1)−Ct angles totaling 354.58°. The Nd(1)−Ga(1)−Ct angle (162.18°) is distorted from linearity. The Ga(1)−Ct distance (1.937 Å) is slightly shorter than that observed in hexameric $(Cp^*Ga)_6$ (2.081 Å).[25] The Nd−Ga bond length in **4** (3.1536(6) Å) is within the expected range based on the sum of their covalent radii (Nd + Ga = 3.23(9) Å) but short relative to the other example of a Nd−Ga bond (3.2199(3) Å).[37] Looking to complexes of Cp*Ga with other lanthanides, $Cp^*_2Eu(GaCp^*)_2$, and $Cp^*_2Yb(THF){-}GaCp^*$ have bond distances (Eu−Ga(1), 3.2499(6); Eu−Ga(2), 3.3907(6); Yb−Ga, 3.2872(4)) which are also longer than the covalent radii sums (Eu + Ga = 3.20(9) Å; Yb + Ga = 3.09(11) Å).[10] Regarding $[(CpSiMe_3)_2Nd(\mu\text{-}OH)]_2$, residual electron density near the oxygen atoms was consistent with bridging hydroxides, and the bond distances and angles compare well with those of $[(CpCMe_3)_2Nd(\mu\text{-}OH)]_2$.

Optical Spectroscopy of 1 and 2. Complexes **1** and **2** present a unique opportunity to explore solution-state electronic structure in a pair of isostructural metal−metal bonded molecules while comparing the effect of group 13 atom coordination. It is important to remember that in solution both **1** and **2** remain in equilibrium with their corresponding starting materials. For this reason optical spectra were shifted onto an arbitrary intensity scale.

The room-temperature optical absorption spectra of **1**, **2**, and the starting material $(CpSiMe_3)_3U$ exhibit a number of broad,

(34) Berthet, J. C.; Lemarechal, J. F.; Nierlich, M.; Lance, M.; Vigner, J.; Ephritikhine, M. *J. Organomet. Chem.* **1991**, *408*, 335–341.
(35) Brennan, J. G.; Andersen, R. A.; Zalkin, A. *Inorg. Chem.* **1986**, *25*, 1756–1760.
(36) (a) Gorden, J. D.; Voigt, A.; Macdonald, C. L. B.; Silverman, J. S.; Cowley, A. H. *J. Am. Chem. Soc.* **2000**, *122*, 950–951. (b) Jutzi, P.; Neumann, B.; Reumann, G.; Schebaum, L. O.; Stammler, H.-G. *Organometallics* **2001**, *20*, 2854–2858.
(37) Arnold, P. L.; Liddle, S. T.; McMaster, J.; Jones, C.; Mills, D. P. *J. Am. Chem. Soc.* **2007**, *129*, 5360–5361.

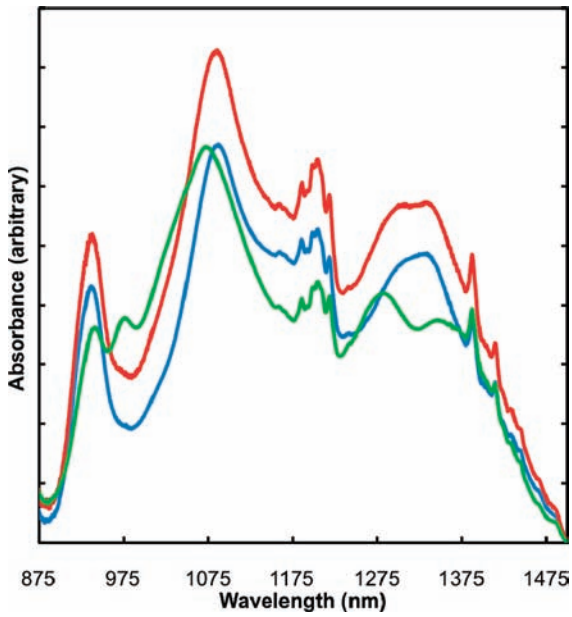

Figure 5. NIR absorption spectrum of 10 mM solutions $(CpSiMe_3)_3U$ (blue), $(CpSiMe_3)_3UAlCp^*$ (**1**, green), and $(CpSiMe_3)_3UGaCp^*$ (**2**, red) C_6H_{12} at room temperature.

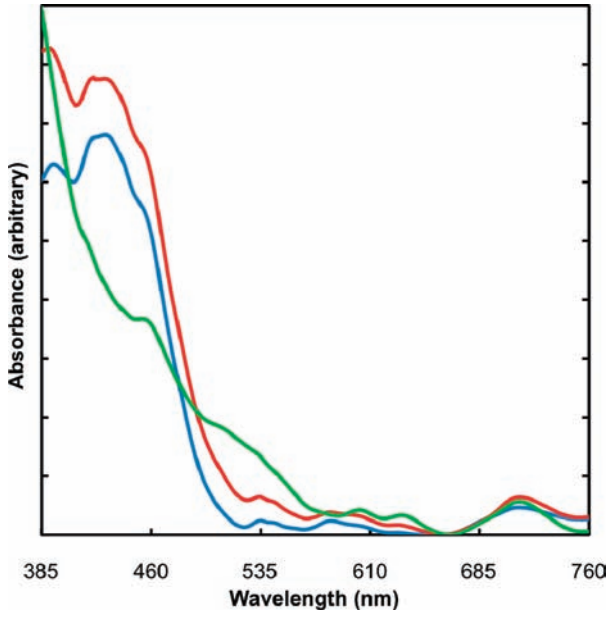

Figure 6. Visible absorption spectrum of 10 mM solutions $(CpSiMe_3)_3U$ (blue), $(CpSiMe_3)_3UAlCp^*$ (**1**, green), and $(CpSiMe_3)_3UGaCp^*$ (**2**, red) C_6H_{12} at room temperature.

intense bands, and a series of well-resolved absorptions in the near-IR region which are characteristic of the Laporte-forbidden $f \rightarrow f$ transitions that are well-known for U(III) coordination compounds (Figure 5). Interestingly, the near-IR regions for **2** and $(CpSiMe_3)_3U$ are nearly identical, although there are significant differences in the bands observed for **1**. In the visible region, **1**, **2**, and $(CpSiMe_3)_3U$ all exhibit a relatively intense band at *ca.* 713 nm. Also in the visible region, two bands observed at *ca.* 603 and 631 nm for **1** are present to a lesser extent in the spectrum of **2** and are virtually absent in $(CpSiMe_3)_3U$ (Figure 6). In addition, a high energy charge-transfer (CT) band is observed at *ca.* 428 nm for **2** and $(CpSiMe_3)_3U$, but it is not discernible in the spectrum of **1**.

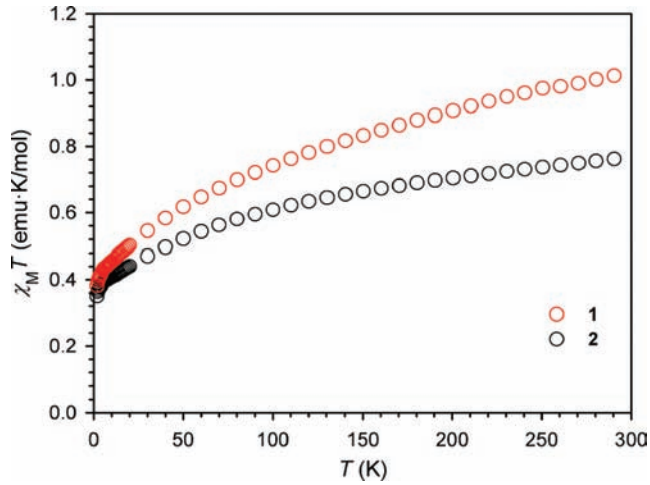

Figure 7. Temperature-dependent $\chi_M T$ plot for **1** and **2** from 1.8 to 300 K.

Though these transitions are not as well resolved, they appear similar to those observed in a related NHC system[38] and are consistent with ^1H and ^{27}Al NMR measurements which indicate that the U−Al interaction in **1** is stronger than that between U−Ga in **2**. Finally, at low concentrations (0.1 mM) the entire spectral band profile for all three molecules is similar, indicating that **1** and **2** are dissociated to their respective starting materials.

Magnetic Susceptibility of 1 and 2. Magnetic exchange interactions between actinide ions have previously been observed in multimetallic complexes,[39] prompting an investigation of the variable-temperature magnetic susceptibility of the isolable U complexes **1** and **2** (Figure 7). The $\chi_M T$ values for **1** drop monotonically from 1.02 emu K mol^{-1} at 300 K to 0.38 emu K mol^{-1} at 1.8 K. The trend followed by **2** is similar; however at 300 K, the $\chi_M T$ value of 0.77 emu K mol^{-1} is considerably lower and declines to 0.35 emu K mol^{-1} at 1.8 K. The magnetic moments at 300 K for **1** (2.86 μ_B) and **2** (2.48 μ_B) also vary from those at 1.8 K for **1** (1.75 μ_B) and **2** (1.67 μ_B). These magnetic moments are substantially lower than the calculated moment for a U(III) ion[40] but well within the range accepted for U(III) coordination compounds.[41]

For both compounds, the decrease in susceptibility with temperature is due to the temperature-dependent variation of the populations of one or more low-lying excited states. Neither compound showed a leveling off of $\chi_M T$ at any temperature indicating that the population of excited states is a significant factor at all temperatures in the studied range. The similarity of the structures of **1** and **2** in the solid state is reflected in the similar trends in the curve of their temperature-dependent magnetic susceptibility. Despite the structural similarity, the significant difference in room temperature moment of **1** and **2** indicates different energies and compositions of their populated excited states, though the similarity of their low temperature moment indicates that they may have the same ground state. Though it is tempting to ascribe the discrepancy in $\chi_M T$ between

(38) Nakai, H.; Hu, X. L.; Zakharov, L. N.; Rheingold, A. L.; Meyer, K. *Inorg. Chem.* **2004**, *43*, 855–857.
(39) Rinehart, J. D.; Harris, D.; Kozimor, S. A.; Bartlett, B. M.; Long, J. R. *Inorg. Chem.* **2009**, *48*, 3382–3395.
(40) Castro-Rodriguez, I.; Olsen, K.; Gantzel, P.; Meyer, K. *J. Am. Chem. Soc.* **2003**, *125*, 4565–4571.
(41) Katz, J. J.; Morss, L. R.; Edelstein, N. M.; Fuger, J. *The Chemistry of the Actinide Elements*, 3rd ed.; Springer: Dordrecht, The Netherlands, 2006; Vol. 1.

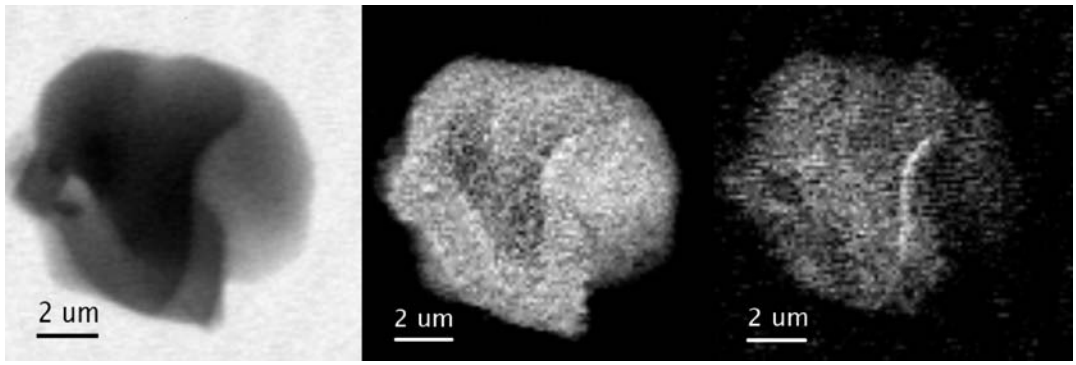

Figure 8. Three images of the particle obtained from powdered **1** material, from which X-ray absorption spectra were collected: normal contrast image obtained with a photon energy of 1558.0 eV (left); elemental map of U obtained by subtraction using photon energies of 728.0 and 737.0 eV with the regions containing U shown as white using a standard grayscale (middle); an elemental map of Al obtained by the same method described for U above with photon energies of 1558.0 and 1567.0 eV with regions containing Al shown as white (right).

1 and **2** to increased orbital overlap with the gallium *p*-orbitals, this is almost certainly an oversimplification of the responsible effects, and further investigation of the solid-state behavior of these complexes is needed.

Scanning Transmission X-ray Spectromicroscopy. Considering the dynamic behavior of complexes **1**−**4** as observed in solution NMR and UV/vis/NIR spectroscopy studies and the difficulty of interpreting the magnetic and X-ray structural data, we sought additional insights with regard to bonding and electronic structure. Ligand K-edge X-ray absorption spectroscopy can provide a quantitative measure of orbital mixing in the ligand−metal bond[42] and has been used successfully to study a series of structurally similar transition metal and actinide metallocene dichlorides.[16b] Scanning transmission X-ray microscopy (STXM) was utilized here to record images, elemental maps, and X-ray absorption near-edge structure (XANES) spectra at the U 4*d*-edges and Al K-edge with the aim of highlighting solid-state geometry and oxidation state differences at the U and Al centers between complex **1** and starting material $(Cp^*Al)_4$.[43] Reproducible measurements were obtained from multiple independently prepared samples.

The radioactive and/or air-sensitive samples were powdered and sealed between two thin (100 nm) silicon nitride windows with epoxy before transfer to the He-purged STXM instrument. The spatial resolution for the U and Al images and spectra were 40 and 50 nm, respectively, and errors in peak energy assignments are 0.040 and 0.125 eV, respectively (refer to the experimental section for complete details). Figure 8 shows a normal contrast image as well as U and Al elemental maps of the particle of **1** from which XANES spectra were recorded. The X-ray images show that the particles from which the spectra were obtained were uniform in composition at the nanometer scale and exhibited no signs of degradation.

The U 4*d*-edge XANES spectrum from **1** is shown in Figure 9 and bears two distinct features which are the atomic-like white line U $4d_{5/2}$ and U $4d_{3/2}$ transitions. The small, broad feature between these two transitions has been observed previously in U spectra independent of oxidation state but has yet to be assigned. These transitions from the U 4*d* orbitals primarily probe unoccupied states with U 5*f* character. The charge state shift of the U $4d_{5/2}$ transition can be used to assign an oxidation state and, considered with the $4d_{3/2}$ transition, can provide additional information on bonding characteristics in some cases.[44]

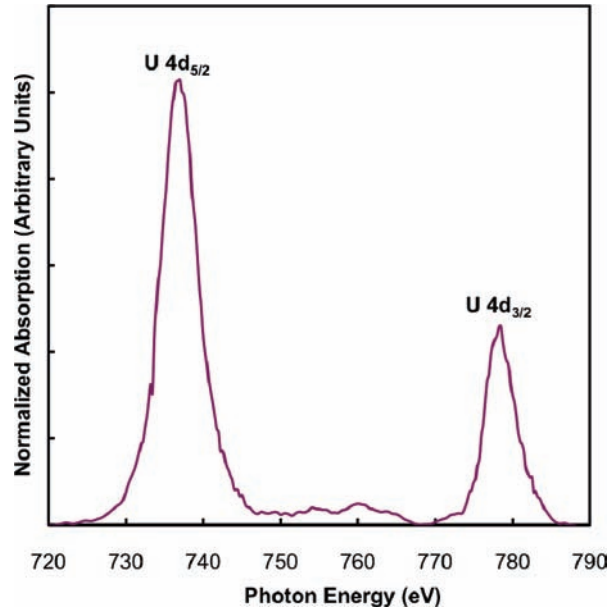

Figure 9. Uranium $4d_{5/2,3/2}$ absorption spectrum collected from the $(CpSiMe_3)_3U-AlCp^*$ (**1**) particle shown in Figure 8.

The U $4d_{5/2}$ and U $4d_{3/2}$ transitions for **1** are found at 736.7 and 778.2 eV, respectively. This compares to the transition energies of 736.6 and 778.3 eV that have been determined for the well-characterized U(III) complex $[U(BBP)_3]I_3$ (BBP = 2,6-bis(2-benzimidazyl)pyridine).[45] A related U(IV) complex, $[U(BBP)_3]Cl_4$, has U 4*d* transitions at 736.9 and 778.4 eV, respectively.[46] More common U(IV) materials such as UCl_4 and UO_2 have $4d_{5/2}$ transitions at 737.1 and 738.5 eV.[44a,46] The lower energy charge state boundary is set by U metal with a U $4d_{5/2}$

(42) Solomon, E. I.; Hedman, B.; Hodgson, K. O.; Dey, A.; Szilagyi, R. K. *Coord. Chem. Rev.* **2005**, *249*, 97–129.
(43) Bluhm, H.; et al. *J. Electron Spectrosc. Relat. Phenom.* **2006**, *150*, 86–104.
(44) (a) Nilsson, H. J.; Tyliszczak, T.; Wilson, R. E.; Werme, L.; Shuh, D. K. *Anal. Bioanal. Chem.* **2005**, *383*, 41–47. (b) Nilsson, H. J.; Tyliszczak, T.; Wilson, R. E.; Werme, L.; Shuh, D. K. In *Proceedings of the Royal Society of Chemistry*; Alvarez, R., Bryan, N. D., May, I., Eds.; Cambridge, U.K., 2006; pp 56−58. (c) Moore, K. T.; van der Laan, G. *Rev. Mod. Phys.* **2009**, *81*, 235–298.
(45) Copping, R.; Teat, S. J.; Janousch, M.; Tyliszczak, T.; Shuh, D. K. In preparation.
(46) Janousch, M.; Copping, R.; Tyliszczak, T.; Castro-Rodriguez, I.; Shuh, D. K. *Mater. Res. Soc. Symp. Proc.* **2008**, *1104*, 165–170.

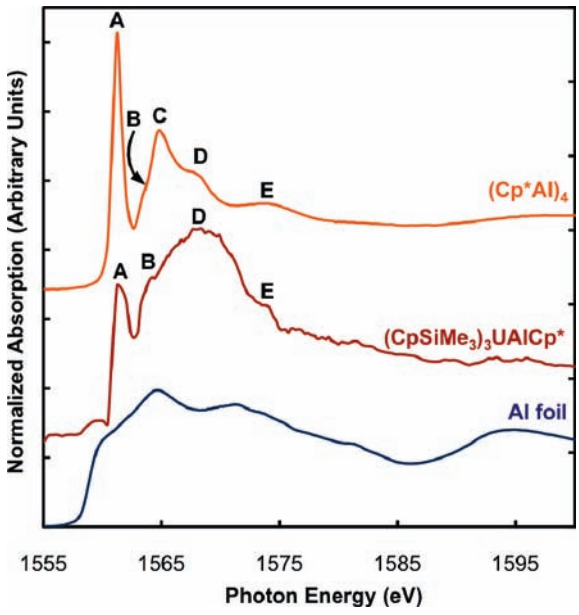

Figure 10. Al K-edge near-edge spectra obtained from a particle of starting material $(Cp^*Al)_4$ (top), $(CpSiMe_3)_3U-AlCp^*$ (**1**) (middle), and a slightly oxidized Al thin film (bottom).

transition at 736.4 eV.[47] The branching ratio ($4d_{5/2}$:$4d_{3/2}$) of **1** is the same as those observed from both the U(III) and U(IV) BBP complexes. The energy position of the U $4d_{5/2}$ transition observed for **1** falls below the energies observed from tested U(IV) materials, above that of metallic U, and in the range established for other formally U(III) materials.

The Al K-edge near-edge spectra recorded from the $(Cp^*Al)_4$ starting material, **1**, and a slightly oxidized Al foil reference are shown in Figure 10. $(Cp^*Al)_4$ provides a prerequisite, unique reference for a formally Al(I) species. The XPS spectrum of $(Cp^*Al)_4$ is known;[48] however we are unaware of any published X-ray absorption spectroscopy studies on such a species. Al K-edge XANES spectroscopy is based on the Al $1s\rightarrow 3p$ transition, which is ideal for the investigation of Al materials.[49] Due to the structural differences between $(Cp^*Al)_4$ and **1**, it is difficult to attribute relative changes in orbital mixing based on the Al K-edge spectra. However, both of the Al complexes in this study have absorption edge positions between those observed for metallic Al (1559.0 eV) and trivalent Al (*ca.* 1565 eV relative to calibration) materials regardless of coordination environment.[50]

The dramatic XANES spectrum of $(Cp^*Al)_4$ has distinct features at 1561.2 (**A**), 1563.8 (**B**), 1565.2 (**C**), 1568.5 (**D**), and about 1574.5 eV (**E**) (Table 3). Most strikingly, the sharp and intense feature **A** in the $(Cp^*Al)_4$ spectrum is shifted to lower energy by *ca.* 4 to 5 eV when compared to four-coordinate Al(III) minerals. This could result from a charge state shift which is characteristic of the Al(I) formal oxidation state and/or from a combination of an Al(I) state and an unusual electronic/structural framework. Feature **A** is also very sharp (1.0 eV fwhm) compared to that observed from known Al(III) species (fwhm 1.5 to 2.0 eV). Considering the known electronic and structural parameters of $(Cp^*Al)_4$, it is prudent to consider **A** a pre-edge feature.

Table 3. Summary of Al K-Edge XANES Spectra Peak Positions and Energy Differences for $(CpSiMe_3)_3UAlCp^*$ (**1**) and $(Cp^*Al)_4$

feature	$(Cp^*Al)_4$ (eV)	difference (eV)	**1** (eV)	difference (eV)	**1** − $(Cp^*Al)_4$ (eV)
A	1561.2	−	1561.6	−	0.4
B	1563.8	2.6	1564.0	2.4	0.2
C	1565.2	1.4	−	−	−
D	1568.5	3.3	1568.7	−	0.2
E	1574.5	6.0	1574.3	5.6	−0.2

An introductory molecular-orbital bonding analysis of $(Cp^*Al)_4$ has been discussed previously.[28,51] The pre-edge feature **A** arises from the combination of the Cp*Al electron pairs which splits the molecular orbitals into $t_2(\pi)$, $e(\pi)$, and $t_1(\pi)$ states, leading to a transition at a lower energy ($t_2(\pi)$: 1561.2 eV, **A**) than would be expected for monomeric Cp*Al [$e(\pi)$: 1563.8 eV, **B** or possibly **C**, 1565.2 eV] which would normally constitute the signature of the Al(I) LUMO.[29b,52] Additional unassigned features are also observed at locations **D** and **E**.

Further evidence for the dative U−Al bond formulation is found in the Al K-edge near-edge spectrum of **1**, shown in Figure 10, which has distinguishable features at 1557.5, 1561.6 (**A**), 1564.0 (**B**), 1568.7 (**D**), and 1574.3 eV (**E**) (Table 3). These features are generally shifted by *ca.* +0.2 eV with respect to their counterparts in the $(Cp^*Al)_4$ spectrum. The intensity of the pre-edge feature **A** in the spectrum of **1** is greatly reduced when compared with that of $(Cp^*Al)_4$, shifted to higher energy (+0.4 eV), and significantly broader (*ca.* 2.0 eV fwhm) and, under close examination, appears to consist of two superimposed, sharp transitions. The reduction in intensity and the very small energy shift likely reflect differences in the molecular orbital mixing and level splittings, which are convoluted by symmetry considerations as the Al coordination in **1** is complex and greatly different than that of $(Cp^*Al)_4$. The large, very broad feature stretching from **B** to nearly **E** is much different in shape than the well-defined features **C** and **D** observed in the spectrum of $(Cp^*Al)_4$ and is likely composed of multiple transitions. By comparison with $(Cp^*Al)_4$, the features in the energy region denoted **B** and **C**−**D**, along with the pre-edge **A**, give strong evidence for an Al(I) species in **1**.

Lastly, the small feature at 1557.5 eV, which was not observed for $(Cp^*Al)_4$, is typically observed in the spectra of nontetrahedral Al(III) and is consistent with dissociation of $(Cp^*Al)_4$ to form a U−Al bond; however in this case it is shifted to correspondingly lower energy. Taken together with the spectrum of $(Cp^*Al)_4$, the Al K-edge near-edge spectrum of **1**

(47) Center for X-ray Optics, X-ray Interactions with Matter, LBNL, Berkeley, CA, USA (http://www-exro.lbl.gov/optical_constants/).
(48) Klemp, C.; Bruns, M.; Gauss, J.; Häussermann, U.; Stösser, G.; van Wüllen, L.; Jansen, M.; Schnöckel, H. *J. Am. Chem. Soc.* **2001**, *123*, 9099–9106.
(49) (a) Dodelet, J. P.; Tourillon, G.; Gastonguay, L.; Cote, R.; Guay, D.; Ladouceur, M.; Flank, A. M.; Lagarde, P. *J. Phys. Chem.* **1992**, *96*, 7202–7206. (b) van Bokhoven, J. A.; van der Eerden, A. M. J.; Koningsberger, D. C. *J. Am. Chem. Soc.* **2003**, *125*, 7435–7442. (c) Balde, C. P.; Mijovilovich, A. E.; Koningsberger, D. C.; van der Eerden, A. M. J.; Smith, A. D.; de Jong, K. P.; Bitter, J. H. *J. Phys. Chem. C* **2007**, *111*, 11721–11725.
(50) (a) McKeown, D. A.; Waychunas, G. A.; Brown, G. E. *J. Non-Cryst. Solids* **1985**, *74*, 349–371. (b) McKeown, D. A. *Phys. Chem. Miner.* **1989**, *16*, 678–683. (c) Li, D. E.; Bancroft, G. M.; Fleet, M. E.; Feng, X. H.; Pan, Y. *Am. Mineral.* **1995**, *80*, 432–440. (d) Ildefonse, P.; Cabaret, D.; Sainctavit, P.; Calas, G.; Flank, A. M.; Lagarde, P. *Phys. Chem. Miner.* **1998**, *25*, 112–121. (e) Yoon, T. H.; Johnson, S. B.; Benzerara, K.; Doyle, C. S.; Tyliszczak, T.; Shuh, D. K.; Brown, G. E. *Langmuir* **2004**, *20*, 10361–10366.
(51) Uhl, W. *Naturwissenschaften* **2004**, *91*, 305–319.
(52) (a) Ahlrichs, R.; Ehrig, M.; Horn, H. *Chem. Phys. Lett.* **1991**, *183*, 227–233. (b) Huber, M.; Schnöckel, H. *Inorg. Chim. Acta* **2008**, *361*, 457–461.

provides evidence of an Al(I) species, and the apparent lack of other pre-edge features confirms the lack of 2*p* character in the principally dative U−Al interaction consisting of Al 2*s* and U 6*d*/5*f* orbitals. We are currently pursuing theoretical methods and examining a series of structurally related complexes so we may further illuminate the electronic structure of these unusual molecules.[53]

Modeling of Metal−Ligand Bond Dissociation Enthalpies. Our inability to experimentally determine [M]−L bond dissociation enthalpies (BDEs) in $(CpSiMe_3)_3M-AlCp^*$ (compounds **1** and **3**, see above), along with a desire to understand the bonding modes in these metal−metal bonded systems, prompted a search for these insights by theoretical methods. Density functional theory has proven very useful in predicting the geometries and electronic structures of lanthanide and actinide complexes[54] as long as their wave functions do not possess strong multiconfigurational character.[55] The extant thermodynamic and kinetic data appear to reproduce experimentally observed reactivity trends,[56] although there is little consensus with respect to the best model chemistries for the *f*-elements or the degree to which the results are consistently reliable.[57] Specifically, while various computations have been reported for Cp_3U-X,[58] to our knowledge calculated U−L BDEs for the dative complexes Cp_3U-L are absent from the literature (except for $(CpR)_3U-CO$)[59] and experimentally determined values are few (see above). Thus, in addition to the new complexes presented here (modeled as Cp_3M-ECp where M = U, Nd and E = Al, Ga), models of six related species comprising Cp_3U-SMe_2, Cp_3U-PMe_3, Cp_3U-THF, Cp_3U-CO, Cp_3U-pyr, and $Cp_3Nd-pyr$ were investigated for a comparison of electronic properties (see below). Two hybrid functionals B3PW91 and B3LYP were used, as well as their GGA ("pure") counterparts BPW91 and BLYP. This should highlight the effects of including exact exchange (HF) and of varying the nature of the correlation functionals. The fifth functional selected was PBE (GGA) which does not use any empirically fitted parameters.

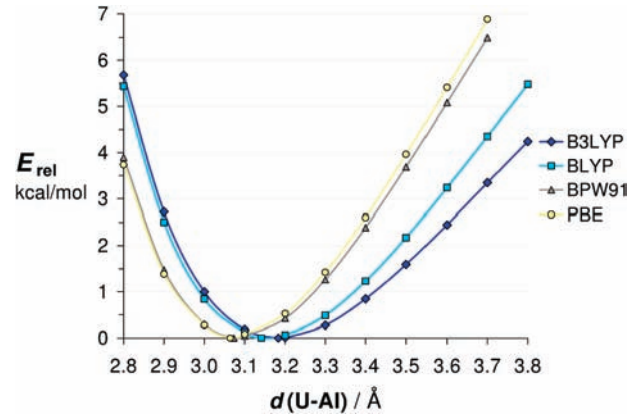

Figure 11. Relaxed coordinate scan of U−Al bond length in H_3U-AlH, 6-31+G(d,p)/SDD basis. The energies were shifted so that the minimum for each curve is at 0 kcal mol^{-1}.

Before discussing these calculations in detail it is pertinent to note that our preliminary computations using a simple H_3U-AlH model indicated that the potential energy wells for the U−Al bond are quite broad for all functionals tested. The results of relaxed coordinate scans of *d*(U−Al) are presented in Figure 11, in which the relative electronic energies were shifted so that the minimum is 0 kcal mol^{-1} in each case. Even in the relatively narrow BPW91 and PBE wells there appears to be available over 0.2 Å of motion within 1 kcal mol^{-1} of the equilibrium U−Al bond length. If this behavior extends to Cp-substituted systems, then assignment of merit for a given functional based on agreement with solid-state experimental bond lengths will be a dubious process as crystal packing forces would be expected to influence the values significantly, as would minor intramolecular steric clashes. This elasticity is evident in the differing M−E bond lengths in the two nonequivalent molecules present in the crystal lattices of **1** and **2**.

Related to this issue is whether the parent Cp is an adequate model for the bulky $SiMe_3$-substituted Cp ligands present in the experimental systems. On steric grounds we posit that it is, mainly because of the relatively broad *d*(M−L) potential profile just discussed. The electronic effects of Cp substitution vary depending on the nature of the ligand L. For instance, the experimental formation enthalpies for the compounds $(CpR)_3M-pyr$ (M = U, Ce) where $R = SiMe_3$ are roughly 4 kcal mol^{-1} larger than those where $R = CMe_3$, although the former set is presumably more sterically crowded.[17c] Conversely, Eisenstein's theoretical work predicts that the [U]−CO BDE decreases by over 7 kcal mol^{-1} when substituting $CpSiMe_3$ for Cp.[59] Unfortunately the fully substituted models proved beyond our computational resources; therefore the lack of Cp substitution and accompanying electronic effects should be considered a potentially serious source of systematic error in the data presented here.

Figure 12 lists the calculated [M]−L bond dissociation enthalpies ΔH_{0K} predicted by each functional for the model compounds Cp_3M-ECp, arbitrarily arranged in order of increasing BDE as calculated using B3LYP. The BDEs for the other dative ligands investigated are presented in the Supporting Information. The PBE functional consistently gave the largest values of those employed, while BPW91 and B3PW91 yielded somewhat smaller values. That the BPW91 GGA and its hybrid version predicted such similar behavior for the uranium complexes is surprising and suggests that issues arising from employing exact exchange in the study of metal−metal bonding

(53) (a) Cabaret, D.; Sainctavit, P.; Ildefonse, P.; Flank, A. M. *J. Phys.: Condens. Matter* **1996**, *8*, 3691–3704. (b) Ankudinov, A. L.; Ravel, B.; Rehr, J. J.; Conradson, S. D. *Phys. Rev. B* **1998**, *58*, 7565–7576. (c) Hay, M. B.; Myneni, S. C. B. *J. Phys. Chem. A* **2008**, *112*, 10595–10603.
(54) (a) Pepper, M.; Bursten, B. E. *Chem. Rev.* **1991**, *91*, 719–741. (b) Vetere, V.; Maldivi, P.; Adamo, C. *J. Comput. Chem.* **2003**, *24*, 850–858. (c) Batista, E. R.; Martin, R. L.; Hay, P. J.; Peralta, J. E.; Scuseria, G. E. *J. Chem. Phys.* **2004**, *121*, 2144–2150. (d) Elkechai, A.; Boucekkine, A.; Belkhiri, L.; Amarouche, M.; Clappe, C.; Hauchard, D.; Ephritikhine, M. *Dalton Trans.* **2009**, 2843–2849. (e) Yahia, A.; Maron, L. *Organometallics* **2009**, *28*, 672–679.
(55) (a) Roos, B. O.; Gagliardi, L. *Inorg. Chem.* **2006**, *45*, 803–807. (b) Lyon, J. T.; Andrews, L.; Malmqvist, P. A.; Roos, B. O.; Yang, T. X.; Bursten, B. E. *Inorg. Chem.* **2007**, *46*, 4917–4925.
(56) (a) Barros, N.; Maynau, D.; Maron, L.; Eisenstein, O.; Zi, G. F.; Andersen, R. A. *Organometallics* **2007**, *26*, 5059–5065. (b) Yang, P.; Warnke, I.; Martin, R. L.; Hay, P. J. *Organometallics* **2008**, *27*, 1384–1392.
(57) Wåhlin, P.; Danilo, C.; Vallet, V.; Réal, F.; Flament, J. P.; Wahlgren, U. *J. Chem. Theory Comput.* **2008**, *4*, 569–577.
(58) (a) Bursten, B. E.; Strittmatter, R. J. *J. Am. Chem. Soc.* **1987**, *109*, 6606–6608. (b) Bursten, B. E.; Rhodes, L. F.; Strittmatter, R. J. *J. Am. Chem. Soc.* **1989**, *111*, 2758–2766. (c) Di Bella, S.; Gulino, A.; Lanza, G.; L., F. I.; Marks, T. J. *J. Phys. Chem.* **1993**, *97*, 11673–11676. (d) Ben Yahia, M.; Belkhiri, L.; Boucekkine, A. *THEOCHEM* **2006**, *777*, 61–73. (e) Elkechai, A.; Boucekkine, A.; Belkhiri, L.; Amarouche, M.; Clappe, C.; Hauchard, D.; Ephritikhine, M. *Dalton Trans.* **2009**, 2843–2849.
(59) Maron, L.; Eisenstein, O.; Andersen, R. A. *Organometallics* **2009**, *28*, 3629–3635.

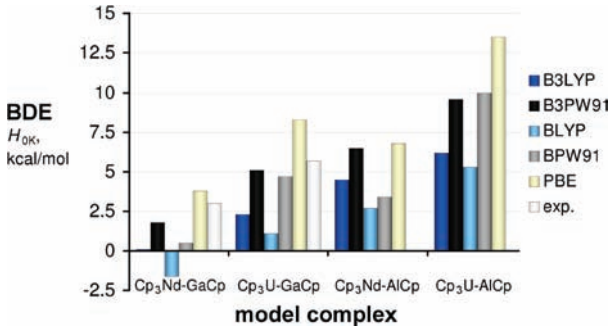

Figure 12. Bond dissociation enthalpies (at 0 K) for the Nd and U model complexes, in order of increasing B3LYP value, at the DFT/BS2//DFT/BS1 level of theory. Experimental values are for $(CpSiMe_3)_3Nd-GaCp^*$ (**4**), $(CpSiMe_3)_3U-GaCp^*$ (**2**).

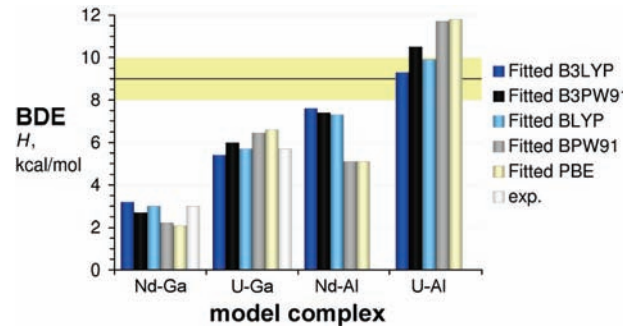

Figure 13. Predicted [M]−L bond dissociation enthalpies (in kcal mol^{-1}) for $(CpSiMe_3)_3Nd-GaCp^*$ (**4**), $(CpSiMe_3)_3U-GaCp^*$ (**2**), $(CpSiMe_3)_3Nd-AlCp^*$ (**3**), and $(CpSiMe_3)_3U-AlCp^*$ (**1**) based on an empirical fitting scheme. The experimental $(Cp^*Al)_4$ BDE value of 9(1) kcal mol^{-1} per Cp*Al is represented by the background yellow region.

are not important here.[60] The values predicted by B3PW91 most consistently matched the experimental BDEs for **2** and **4**, although it cannot be concluded that this is the most accurate functional here because the comparisons are with simplified models. Finally, both BLYP and B3LYP clearly underestimated the BDE values, and thus it appears that the LYP correlation functional is not well suited for these and similar systems.

The agreement between the BDE values calculated by each functional for each of the CpAl and CpGa species is quite poor; however the difference in BDE between each complex is fairly consistent across all five model chemistries. A qualitative inconsistency is that the BPW91 and PBE functionals predicted a slightly larger [M]−L BDE for $Cp_3U-GaCp$ than for $Cp_3Nd-AlCp$, in contrast to the other three methods. That being stated, it is probable that the use of isostructural models in this case results in sufficiently systematic DFT errors that an empirical correction can be applied in order to estimate the [M]−L BDEs for Cp*Al compounds **1** and **3**. This approach is not unreasonable considering that vibrational frequencies are routinely scaled to fit experiment and even the functionals themselves contain empirically fitted parameters. For each functional, the difference in [M]−L BDEs was taken between that calculated and that experimentally derived (for **2** and **4**). The differences for the Nd and U systems were then averaged in an attempt to remove any bias introduced by random errors present in the data, and finally these averaged correction factors were added to the calculated values for each functional. Figure 13 depicts the result of this process.

Not surprisingly, each fitted value for the Ga-containing complexes closely matches the experimental value, as these were used in the fitting process. It should be stressed, however, that such agreement exists when using a fit based on the Nd/U average correction. The result is that fitted BDE values for the $Cp_3Nd-GaCp$ and $Cp_3U-GaCp$ models where the raw values are more mutually consistent will agree better with experiment than those where the raw values differ, as in the BPW91 and PBE data. These per-functional corrections were added to the $Cp_3M-AlCp$ BDE values under the assumption that the fitting value does not depend on the species of group 13 element. In defense of this assumption we point out that the $Cp_3M-AlCp$ fitted values (for three of the five functionals) agree very well with the noncorrected B3PW91 values, which for the $Cp_3M-GaCp$ set apparently predict the experimental values most consistently. The relative success of this functional prompted us to attempt the modeling of the substituted diyl complexes Cp_3U-ECp^* (E = Al, Ga), and [M]−L BDE values of 10.2 and 6.0 kcal mol^{-1} (respectively) were derived (vs 9.6 and 5.1 kcal mol^{-1} for the unsubstituted models). Therefore, the diyl Cp* methyl groups of the experimental systems do not appear to greatly affect the [M]−L BDEs by either steric or electronic means, and thus the simplification of the CpE ligands is not a major source of error.

From extrapolation of the fitted data we find that, depending on the functional used, the [M]−L BDE for **3** falls in the range 5.1−7.6 kcal mol^{-1} while that for **1** is 9.3−11.8 kcal mol^{-1}. Provided the experimentally determined $(CpSiMe_3)_3U-THF$ BDE value[32] of 9.8(1) kcal mol^{-1} is accurate and has the reported precision, then the observation that THF at least partially displaces Cp*Al in **1** (see above) rules out the BPW91 and PBE values. Averaging the fitted BDEs for the remaining three functionals yielded the values 7.4 and 9.9 kcal mol^{-1} for **3** and **1**, respectively, which we propose as our best estimates given the data presented here. To reiterate, the experimentally estimated BDE for $(Cp^*Al)_4$ is 9(1) kcal mol^{-1} per Cp*Al monomer. Regardless of the chosen functional, our results are consistent with the fact that formation of **1** is energetically competitive with the formation of $(Cp^*Al)_4$, and they suggest an upper bound for its [M]−L BDE. Furthermore, no tested model chemistry yielded values predicting that the BDE for **3** is sufficiently large for that compound to be isolable. While experiment does suggest that **3** can exist in low concentrations, the proposed BDE is in acceptable agreement with the relative energies involved in such an equilibrium. Due to the competing formation of $(Cp^*Al)_4$, this system represents an unusual example of a ligand approaching ideal selectivity for an actinide over the corresponding lanthanide.

Electronic Analysis of Metal−Ligand Bonding in Cp_3M-L. According to the experimental evidence and the predicted BDEs presented above, compound **1** has an Al→U dative bond that is nearly as strong as the O→U bond in $(CpSiMe_3)_3U-THF$. The small electronegativity difference between U and Al suggests that the ionic component of bonding between these elements should be small, and therefore a relatively large covalent contribution is necessarily invoked. This proposal is supported by results from a Natural Bond Orbital (NBO) analysis on the 10 geometrically optimized species presented above. This type of treatment has been proven to yield

(60) (a) Barden, C. J.; Rienstra-Kiracofe, J. C.; Schaefer, H. F., III. *J. Chem. Phys.* **2000**, *113*, 690–700. (b) Schultz, N. E.; Zhao, Y.; Truhlar, D. G. *J. Phys. Chem. A* **2005**, *109*, 4388–4403. (c) Furche, F.; Perdew, J. P. *J. Chem. Phys.* **2006**, *124*, 044103.

reasonable data for the actinides,[56b,61] provided that the 6*d* subshell is included in the valence space.[62] Because in some instances the analysis assigned a U−L bonding NBO and in others the interactions were included via delocalizations, we found that the relevant interactions were most easily inspected using the Natural Localized Molecular Orbital (NLMO)[63] formalism in which the delocalization tails are included in each orbital. The B3PW91 functional was employed in these studies because it yielded BDE values closest to those predicted for the Cp*Al and Cp*Ga complexes (see disclaimer above). The most relevant quantities derived from this analysis are summarized in Table 4, with the B3PW91-predicted BDE values for purposes of comparison.

The Natural Localized Molecular Orbital/Natural Population Analysis (NLMO/NPA) bond orders[64] are used here as a measure of the covalent character of each dative bond. According to these data, the U−Al bond in Cp_3U−AlCp exhibits the most covalent character of the set (BO = 0.754), while the M−L bonds in Cp_3U−GaCp and Cp_3U−CO have slightly less. The uranium centers in these three species have relatively small (natural) partial positive charges which indicate diminished ionic bonding character. While comparisons between the Nd and U based on metal charge are difficult, the NLMO/NPA bond orders suggest that the U−Ga bond should actually be stronger than that of the neodymium analogue. Thus, the BDE ordering based on the BPW91 and PBE results may be more appropriate (note that this would in turn suggest a larger difference in [M]−L BDEs between the Nd−Al and U−Al complexes; see above).

Orbital contributions are apparently much less important in metal−ligand bonding with the hard Lewis bases such as THF and pyridine; the relatively large partial charges on the uranium centers of those two complexes indicate significant ionic bonding character. The most favorable bonding situation occurs when considerable orbital *and* ionic bonding contributions are present, as in the case of Cp_3U−PMe_3 and to a lesser extent in Cp_3U−pyr. The uranium partial charge and NLMO/NPA bond order in Cp_3U−CO closely match those of Cp_3U−AlCp. The experimentally observed analogues have similar [M]−L BDEs, and so it is likely that this analysis, while yielding a more qualitative ordering of [M]−L BDEs, does not suffer from some of the factors resulting in grossly spurious directly calculated BDEs (see the Supporting Information).

While charge and bond order analyses predicted that the bonding between uranium and CO or CpAl is primarily covalent and of similar extent, they state nothing regarding the specific interactions from which the covalency arises. Columns 5 and 6 of Table 4 list the percentage of the ligand's σ-type lone-pair electron density donated to the metal and the percentage of the metals π-type SOMO electron density back-donated to the ligand, respectively. For Cp_3U−GaCp, Cp_3U−AlCp, and Cp_3U−CO, the NBO/NLMO analysis assigned an actual U−E bond (E = Ga, Al, C) with coefficients corresponding to the

Table 4. Relevant B3PW91 Data from NBO/NLMO Analysis of Optimized Cp_3M−L, Concerning the Nature of [M]−L Bonding (the Entries Are Ordered for Consistency with the above Figures)

[M]−L complex[a]	BDE[b] (kcal/mol)	NC(M)[c]	NLMO/NPA BO(M−E[d])[e]	%LP(E_σ)→M_σ[f]	%SOMO(M_π) →L
[Nd]−GaCp	1.8	1.108	α 0.201	α 13.5	*x* 0.1
			β 0.192	*β* 12.6	*y* 0.1
			total 0.393	**average 13.0**	**average 0.1**
[U]−GaCp	5.1	0.548	α 0.342	α 23.1	*x* 1.1
			β 0.297	*β* 20.9	*y* 1.1
			total 0.639	**average 22.0**	**average 1.1**
[Nd]−AlCp	6.5	1.038	α 0.229	α 17.5	*x* 0.0
			β 0.212	*β* 16.2	*y* 0.0
			total 0.441	**average 16.8**	**average 0.0**
[U]−AlCp	9.6	0.441	α 0.410	α 30.1	*x* 1.5
			β 0.344	*β* 27.2	*y* 1.5
			total 0.754	**average 28.6**	**average 1.5**
[U]−SMe_2	9.8	0.792	α 0.143	α 13.6(1.5)	*x* 0.4
			β 0.135	*β* 12.8(1.5)	*y* 0.1
			total 0.278	**average 13.2**	**average 0.2**
[Nd]−pyr	10.1	1.323	α 0.076	α 6.2	*x* 0.1
			β 0.071	*β* 5.9	*y* 0.1
			total 0.147	**average 6.1**	**average 0.1**
[U]−THF	10.1	0.985	α 0.070	α 5.9(1.2)	*x* 0.1
			β 0.072	*β* 5.6(1.3)	*y* 0.1
			total 0.143	**average 5.8**	**average 0.1**
[U]−PMe_3	14.2	0.728	α 0.200	α 18.3	*x* 0.2
			β 0.191	*β* 17.1	*y* 0.2
			total 0.391	**average 17.7**	**average 0.2**
[U]−pyr	13.1	0.961	α 0.109	α 8.1	*x* 3.2
			β 0.092	*β* 7.5	*y* 0.1
			total 0.202	**average 7.8**	**average 1.7**
[U]−CO	(17.2)[g]	0.599	α 0.427	α 21.3	*x* 9.7
			β 0.267	*β* 20.7	*y* 9.7
			total 0.694	**average 21.0**	**average 9.7**

[a] [M] = Cp_3M. [b] [M]−Ligand bond dissociation enthalpy, ΔH_{0K} at B3PW91/BS2//B3PW91/BS1 level of theory. [c] Natural charge on M. [d] L atom bound to M. [e] Natural Localized Molecular Orbital/Natural Population Analysis Bond Order. [f] Second ligand donor lone pair in parentheses and not included in average. [g] This value should be disregarded.

σ-donation data presented in Table 4. The values for ligand-to-metal σ donation correlate with the NLMO/NPA bond orders (except for Cp_3U−CO), as this interaction is primarily responsible for covalent bonding in these cases. Before discussing these interactions further, the NBO/NLMO results will be related to the standard MO theory. Figure 14 depicts the two molecular orbitals that can be thought of as having the highest contribution from the M−E σ-bonding NBOs in Cp_3U−GaCp, Cp_3U−AlCp, and Cp_3U−CO. Canonical molecular orbital analyses show that the lower-energy MOs (Figure 14, left) have 89%, 86%, and 79% bonding character in Cp_3U−GaCp, Cp_3U−AlCp, and Cp_3U−CO, respectively, while the percent bonding characters due to the M−E σ-bonding NBO in each are 66%, 62%, and 38%. The higher-energy MOs possessing the largest contribution from the M−E NBO (after those discussed above) are shown on the right of Figure 14. That of the gallium model has only a 6% contribution from the U−Ga bonding NBO, while the U−Al NBO contributes 20% of the net bonding interaction (75% bonding overall) in that Cp_3U−AlCp MO. The minor interactions involving the U−C σ-bonding NBO of Cp_3U−CO

(61) (a) Cantat, T.; Graves, C. R.; Jantunen, K. C.; Burns, C. J.; Scott, B. L.; Schelter, E. J.; Morris, D. E.; Hay, P. J.; Kiplinger, J. L. *J. Am. Chem. Soc.* **2008**, *130*, 17537–17551. (b) Cantat, T.; Arliguie, T.; Noël, A.; Thuéry, P.; Ephritikhine, M.; Le Floch, P.; Mézailles, N. *J. Am. Chem. Soc.* **2009**, *131*, 963–972.
(62) Clark, A. E.; Sonnenberg, J. L.; Hay, P. J.; Martin, R. L. *J. Chem. Phys.* **2004**, *121*, 2563–2570.
(63) (a) Reed, A. E.; Weinhold, F. *J. Chem. Phys.* **1985**, *83*, 1736–1740. (b) Hübler, K.; Hunt, P. A.; Maddock, S. M.; Rickard, C. E. F.; Roper, W. R.; Salter, D. M.; Schwerdtfeger, P. *Organometallics* **1997**, *16*, 5076–5083.
(64) Reed, A. E.; von Ragué Schleyer, P. *J. Am. Chem. Soc.* **1990**, *112*, 1434–1445.

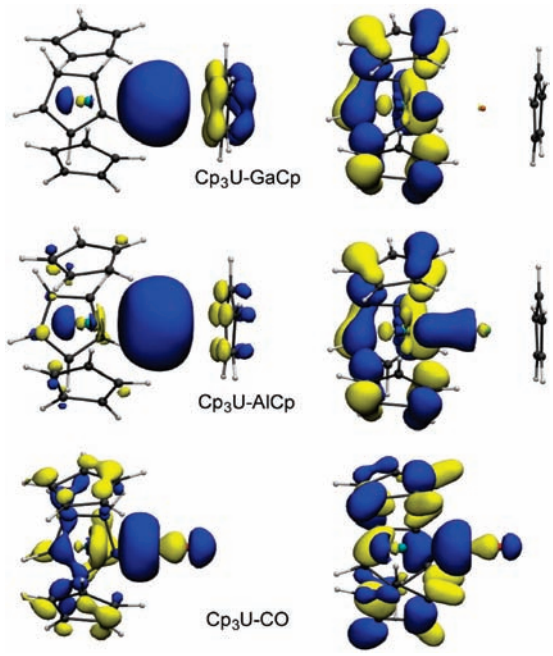

Figure 14. Diagrams of primary uranium−ligand bonding σ-bonding molecular orbitals of $Cp_3U-GaCp$ (top), $Cp_3U-AlCp$ (center), and Cp_3U-CO (bottom), at identical isovalues, computed with B3PW91/BS2//B3PW91/BS1. The orbitals on the left are lower in energy than those on the right.

are spread out over more MOs, but said NBO contributes 20% of the total 89% bonding character of the Cp_3U-CO MO depicted in Figure 14 (right).

Returning to the data presented in Table 4, 28.6% of the electron density in the U−Al σ-bonding NLMO is centered on uranium; in other words the CpAl fragment donates almost 30% of its lone-pair electron density to the uranium center. In the CpGa case the σ donation is little more than two-thirds as strong at 22.0%, while in the CO complex it is slightly smaller still (21.0%). The hybridization of the CpE donor lone pair in Cp_3UECp is 92% *s* where E = Al and 96% *s* where E = Ga. An explanation for this decrease in lone-pair donation can be found in the energy levels of these donor orbitals in the free CpE ligands, which are mostly of *s* character at E and are antibonding with respect to the Cp π-system. This lone pair in CpAl is the HOMO, with an orbital energy of −5.98 eV. In contrast, the corresponding orbital in CpGa is at −6.97 eV which places it below the (degenerate) Cp→Ga orbitals of π symmetry. This phenomenon is presumably due to the "transition series contraction"[65] which arises from incomplete shielding of the Ga nucleus by the 3*d* electrons. This relative lone-pair destabilization in CpAl apparently renders the ligand's donor orbital slightly more diffuse than that of CpGa, as can be observed upon close inspection of the MO diagrams in Figure 14. The donor orbital of CO is obviously more compact and lower in energy than either of these two (−10.5 eV in this model chemistry).

Why does a diffuse donor orbital result in a stronger covalent bond with uranium? Table 5 lists the electronic configuration and σ-acceptor orbital hybridization at the U or Nd centers of each complex presented, as derived from the NBO/NLMO analysis. For the U complexes, the metal orbitals that are more

(65) Mingos, D. M. P. *Essential Trends in Inorganic Chemistry*; Oxford University Press: Oxford, 1998.

Table 5. U/Nd Electron Configurations and Acceptor Orbital Hybridizations

[M]−L complex[a]	M electronic config.[b]	L→M σ-acceptor hybrid[c]
[Nd]−GaCp	$6s^{0.18}4f^{3.16}5d^{1.52}$	21.5%*s* 75.1%*d* 3.2%*f*
[U]−GaCp	$7s^{0.23}5f^{3.38}6d^{1.66}$	18.4%*s* 66.8%*d* 14.8%*f*
[Nd]−AlCp	$6s^{0.20}4f^{3.17}5d^{1.55}$	22.8%*s* 73.5%*d* 3.5%*f*
[U]−AlCp	$7s^{0.26}5f^{3.36}6d^{1.77}$	19.4%*s* 67.6%*d* 13.0%*f*
[U]−SMe_2	$7s^{0.20}5f^{3.44}6d^{1.35}$	18.8%*s* 61.3%*d* 19.8%*f*
[Nd]−pyr	$6s^{0.15}4f^{3.18}5d^{1.31}$	18.1%*s* 76.6%*d* 5.1%*f*
[U]−THF	$7s^{0.17}5f^{3.42}6d^{1.21}$	18.8%*s* 56.6%*d* 24.5%*f*
[U]−PMe_3	$7s^{0.22}5f^{3.43}6d^{1.42}$	19.2%*s* 63.0%*d* 17.8%*f*
[U]−pyr	$7s^{0.17}5f^{3.40}6d^{1.25}$	15.6%*s* 61.1%*d* 23.0%*f*
[U]−CO	$7s^{0.22}5f^{3.36}6d^{1.64}$	15.6%*s* 60.9%*d* 23.2%*f*

[a] B3PW91/BS2//B3PW91/BS1, [M] = Cp_3M. [b] 0.05 electron cutoff. [c] 0.2% cutoff, α spin orbital only.

populated in the presence of strong σ donors are the 7*s* and the especially diffuse 6*d* subshells. In contrast, what electron density exists on the metal center in the more ionic cases such as Cp_3U-THF is concentrated in the more compact 5*f* orbitals. Thus a high-energy, diffuse ligand lone pair can be greatly stabilized by interacting with the relatively low-lying and formally empty *s* and *d* subshells on the U(III) ion. Interestingly, the percentage of *f* orbital character in the metal acceptor hybrid increases as the ligand donor orbital becomes more compact, partially compensating for the resulting orbital size mismatch. For example, while L→M σ donation in $Cp_3U-GaCp$ and Cp_3U-CO is nearly identical in magnitude, the U−centered acceptor hybrid is only 14.8% *f* in the former but 23.2% *f* in the latter. These data suggest that in low-valent uranium the availability of the 5*f* orbitals provides an extra degree of flexibility in bonding with various ligand types. This effect is not observed in the neodymium species, where 4*f* participation is comparable (and quite small) in $Cp_3Nd-pyr$ and $Cp_3Nd-AlCp$.

As one would expect, the lanthanide complexes and those uranium complexes containing poor π-acceptors engage in virtually no metal-to-ligand back-donation (Table 4, column 6). We had anticipated, however, that the relatively diffuse uranium 5*f*-centered SOMOs of the proper symmetry for M→L back-donation from Cp_3U could interact significantly with the formally empty, π-symmetric aluminum or gallium-centered *p* orbitals in CpE. In fact, according to these calculations the uranium π-SOMO → Al/Ga *p*-orbital donation is negligible. The situation is somewhat different in Cp_3U-CO, however, wherein its π-type SOMOs possess a significant contribution from the CO π^* MOs as depicted in Figure 15. It is this 9.7% back-donation that accounts for the similar overall NLMO/NPA bond orders in $Cp_3U-AlCp$ and Cp_3U-CO. The right portion of Figure 15 shows a superposition of the uranium-centered SOMOs (depicted in the left portion) and the virtual orbital primarily consisting of the ligand π-acceptor orbitals in $Cp_3U-GaCp$ and $Cp_3U-AlCp$. It is obvious from these drawings that these actinide-centered *f* orbitals are quite compact even though they are singly occupied and, thus, do not overlap well with the CpE ligand acceptor orbitals.

In summary, the computational results indicate that CpAl and CpGa ligands behave somewhat like heteroatom-stabilized carbenes in that they are good σ-donors but poor π-acceptors, even though they possess formally empty *p* orbitals of the proper symmetry for π back-donation. The principal differences are that the donor lone pairs are quite diffuse and bonding interactions with electropositive metals have comparatively little ionic character. Therefore, in accordance with the most recent

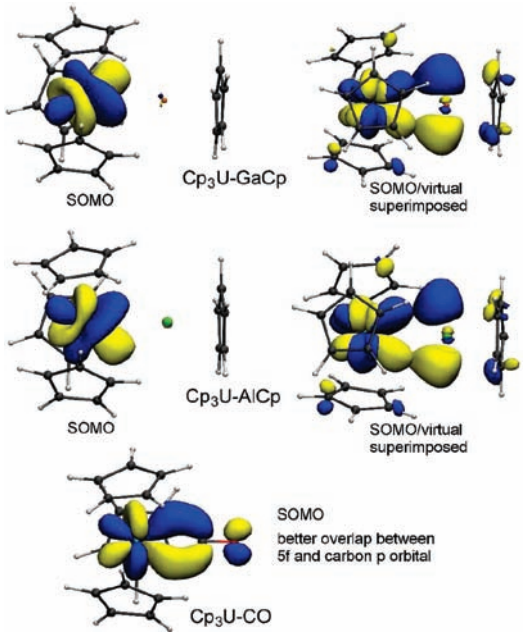

Figure 15. Diagrams of molecular orbitals involved in uranium−ligand p-bonding in $Cp_3U-GaCp$ (top), $Cp_3U-AlCp$ (center), and Cp_3U-CO (bottom), at identical isovalues, computed with B3PW91/BS2//B3PW91/BS1. The orbitals on the right are composite drawings of a uranium-centered SOMO and a primarily ligand-centered virtual orbital of π symmetry.

theoretical data on $(CpR)_3U-CO$,[59] it appears that the 4*f*/5*f* selectivity observed for these ligands must be rationalized using differences in metal σ-acceptor ability rather than by invoking π-orbital back-donation.

Conclusion

We have observed four new *f*-element metal−metal bonded complexes of the group 13 diyls, $(CpSiMe_3)_3M-ECp^*$ (**1**: M = U, E = Al; **2**: M = U, E = Ga; **3**: M = Nd, E = Al; **4**: M = Nd, E = Ga). Both uranium compounds **1** and **2** have been structurally characterized and can be prepared in moderate to good yields on multigram scales. The observed metal−metal bond distances are short, although DFT calculations suggest that the potential energy well for U−Al bonding is very shallow, and distances may be strongly influenced by intermolecular forces.

These results also provide an unprecedented opportunity to compare 4*f* and 5*f* reactivity and observe group 13 trends, in a series of isostructural and isoelectronic metal−metal bonded compounds. The $(CpSiMe_3)_3Nd/(CpSiMe_3)_3U$ system provides convenient entry into the synthesis and detailed characterization of 4*f* and 5*f* interactions with weakly coordinated small molecules. In this context we have shown by DFT calculations that Cp*Al is a slightly better donor than Cp*Ga, while quantitative ^{1}H NMR studies reveal that U is a better acceptor for soft σ-donating ligands than Nd by an order of magnitude. Through ^{1}H NMR competition experiments, it was shown that Cp*Al and Cp*Ga are both capable of binding 5*f* over 4*f* elements with excellent selectivity, though DFT calculations suggest that the origin of this selectivity arises principally from the strong σ-interaction and is not due to stabilization of the U 5*f* electrons through π-backbonding.

Structural, magnetic, spectroscopic, and computational characterization reveals multiple components to the bonding interactions in this series of compounds. For Nd complexes **3** and **4**, the bonding is weak and predominantly electrostatic; however a minimal amount of lone-pair σ-donation from Al or Ga onto Nd is observed. The metal−metal bonding in U complexes **1** and **2** arises predominantly from Al or Ga lone-pair σ-donation onto U; weak electrostatic interactions are observed, and a vanishingly small amount of U π-electron density is donated into the formally empty π-symmetric *p* orbitals on Al or Ga. In the simplest sense, Cp*Al and Cp*Ga behave analogously with N-heterocyclic carbenes, i.e. good σ-donors with a limited capacity for π-acceptance.

These results, especially taken together with a report of Ga σ and π-donation in a U(IV) complex,[12] suggest that the 5*f* orbitals improve the σ-bonding flexibility of the U atom with different types of ligands. Further synthetic and reactivity studies, as well as evaluation of improved computational methods, are currently ongoing.

Experimental Section

General Considerations. All reactions were performed using standard Schlenk-line techniques or in an MBraun drybox (<1 ppm O_2/H_2O) unless noted otherwise. All glassware was dried at 150 °C for at least 12 h or flame-dried under vacuum prior to use. Tetrahydrofuran, toluene, diethyl ether, *n*-pentane, and *n*-hexane were purified by passage through a column of activated alumina,[66] stored over sodium/benzophenone, and vacuum transferred immediately prior to use. Deuterated toluene, benzene, and cyclohexane were vacuum transferred from NaK/benzophenone. NMR spectra were recorded at ambient temperature (unless otherwise indicated) on a Bruker DRX-500 spectrometer. ^{1}H chemical shifts are given relative to residual solvent peaks, and coupling constants (*J*) are given in Hz. ^{27}Al NMR chemical shifts are referenced to an external standard of 1 M $Al(NO_3)_3$ in H_2O/D_2O (δ 0 ppm). Infrared samples were prepared as Nujol mulls and taken between KBr disks. Samples for ultraviolet, visible, and near-infrared spectrometry were prepared in a Schlenk-adapted quartz cuvette and analyzed on a Shimadzu UV-3101PC scanning spectrophotometer. Melting points were determined using sealed capillaries prepared under nitrogen and are uncorrected. $(Cp^*Al)_4$,[67] Cp*Ga,[30] and $(CpSiMe_3)_3U$[35] were prepared according to literature procedures. Unless otherwise noted, all other reagents were acquired from commercial sources and used as received. Elemental analyses were determined at the Microanalytical Laboratory of the College of Chemistry, University of California, Berkeley. X-ray structural determinations were performed at CHEXRAY, University of California, Berkeley.

Crystallographic Analysis. Single crystals of **2**,[68] $(CpSiMe_3)_3Nd$,[69] and **4** + $[(CpSiMe_3)_2Nd(\mu\text{-}OH)]_2$[70] were coated in Paratone-N oil, mounted on a Kaptan loop, transferred to a Bruker APEX CCD area detector, centered in the beam, and cooled by a

(66) Alaimo, P. J.; Peters, D. W.; Arnold, J.; Bergman, R. G. *J. Chem. Educ.* **2001**, *78*, 64–64.
(67) Schormann, M.; Klimek, K. S.; Hatop, H.; Varkey, S. P.; Roesky, H. W.; Lehmann, C.; Röpken, C.; Herbst-Irmer, R.; Noltemeyer, M. *J. Solid State Chem.* **2001**, *162*, 225–236.
(68) Crystal data for **2**: $C_{34}H_{54}GaSi_3U$, M_r = 854.79, T = 153(2) K, monoclinic, space group *Pc*, a = 16.4174(10) Å, b = 12.8384(8) Å, c = 17.5249(11) Å, β = 90.1740(10)°, V = 3693.8(4) Å^3, μ = 5.226 cm^{-1}, Z = 4, 20 717 reflections measured, 10 013 unique (R_{int} = 0.0556), final R indicies [$I > 2\sigma(I)$] $R(1)$ = 0.0516, w$R2$ = 0.0820.
(69) Crystal data for $(CpSiMe_3)_3Nd$: $C_{24}H_{39}NdSi_3$, M_r = 556.06, T = 130(2) K, orthorhombic, space group *Pbca*, a = 8.3245(5) Å, b = 22.2396(12) Å, c = 28.9822(16) Å, $\alpha = \beta = \gamma$ = 90.00°, V = 5365.6(5) Å^3, μ = 2.077 cm^{-1}, Z = 8, 29 257 reflections measured, 5506 unique (R_{int} = 0.0687), final R indicies [$I > 2\sigma(I)$] $R(1)$ = 0.0349, w$R2$ = 0.0691.
(70) Crystal data for **4** + $(CpSiMe_3)_2Nd(\mu\text{-}OH)$: $C_{50}H_{81}GaNd_2OSi_5$, M_r = 1196.80, T = 131(2) K, monoclinic, space group *P*1, a = 13.1352(10) Å, b = 13.1883(10) Å, c = 17.8240(13) Å, α = 90.5800(10)°, β = 103.0090(10)°, γ = 109.1190(10)°, V = 2830.7(4) Å^3, μ = 2.417 cm^{-1}, Z = 2, 18 504 reflections measured, 11 362 unique (R_{int} = 0.0301), final R indicies [$I > 2\sigma(I)$] $R(1)$ = 0.0393, w$R2$ = 0.0882.

nitrogen flow low-temperature apparatus that had been previously calibrated by a thermocouple placed at the same position as the crystal. Preliminary orientation matrices and cell constants were determined by collection of 60 30-s frames, followed by spot integration and least-squares refinement. An arbitrary hemisphere of data was collected, and the raw data were integrated using SAINT.[71] Cell dimensions reported were calculated from all reflections with $I > 10\sigma$. The data were corrected for Lorentz and polarization effects, but no correction for crystal decay was applied. Data were analyzed for agreement and possible absorption using XPREP.[72] An empirical absorption correction based on comparison of redundant and equivalent reflections was applied using SADABS.[73] The structures were solved using SHELXS[74] and refined on all data by full-matrix least-squares with SHELXL-97.[75] Thermal parameters for all non-hydrogen atoms were refined anisotropically. Residual electron density in the difference Fourier map was assigned to O−H bonds in **4** + $[(CpSiMe_3)_2Nd(\mu\text{-}OH)]_2$, and the associated proton positions were refined with an isotropic displacement parameter of 1.5 times the parent atom. The Cp* ligand in **4** is disordered; two rings with accompanying methyl groups were created with identical geometries and refined anisotropically with occupancy factors constrained to sum to unity. In addition, the $SiMe_3$ group attached to C11 in **4** is also disordered; two $SiMe_3$ groups were created with identical geometries and refined anisotropically with occupancy factors constrained to sum to unity. ORTEP diagrams were created using the ORTEP-3 software package and POV-Ray.[76]

Computational Details. All structures and energies were calculated using the Gaussian03[77] suite of programs. Self-consistent field computations were performed with tight convergence criteria on ultrafine grids, while geometry optimizations were converged to at least the default geometric convergence criteria. In some instances it was necessary to use the quadratic convergence method to achieve SCF convergence.[78] All Nd and U complexes were modeled with the unrestricted formalism and were assumed to be quartets, with three unpaired electrons. These complexes never exhibited $\langle S^2 \rangle$ values greater than ~3.77 so spin contamination is not an issue here. The Al and Ga monomers were examined in both their singlet and triplet states, and the singlet was found to be the ground state for each. The use of symmetry was explicitly turned off for all computations. Frequencies were calculated analytically at 298.15 K and 1 atm, and structures were considered true minima if they did not exhibit imaginary modes with frequencies greater than $15i$ cm^{-1}. The GGA functionals used were BLYP,[79] BPW91,[79a,80] and PBE,[81] and the hybrid functionals were B3LYP[79,82] and B3PW91.[79a,80,83] Stuttgart-type small core ECPs and their appropriate valence basis sets were used for Ga,[84] Nd,[85] and U,[86] with valence contraction schemes (11*s*12*p*10*d*2*f*)/[6*s*5*p*4*d*2*f*], (14*s*13*p*-10*d*8*f*6*g*)/[10*s*8*p*5*d*4*f*3*g*], and (14*s*13*p*10*d*8*f*6*g*)/[10*s*9*p*5*d*4*f*3*g*], respectively. Note that the valence bases used for Ga and U were those taken from their Web site[87] rather than those included in the Gaussian code. For geometry optimizations and frequency calculations, the remaining atoms were treated with Pople's 6-31G(d) double-ζ split-valence basis,[88] except for the (non-Cp) ligand atom that would bind the metal, which was treated with the triple-ζ 6-311+G(d) basis.[89] This combination is referred to here as BS1. Single-point energy calculations were performed on all optimized structures wherein all atoms not using ECPs were treated with the 6-311+G(d,p) basis (referred to as BS2), and the zero-point energies calculated at BS1 were added to those to obtain 0 K [M]−L bond dissociation enthalpies. BDEs obtained in this manner were up to ca. 2 kcal mol^{-1} lower than those calculated using only BS1, presumably due to a mitigation of basis set superposition error. Natural Bond Orbital analyses were performed as follows: NBO archive files were generated by Gaussian's built-in NBO3.1.[90] These files were then used as input for a modified version of the standalone GENNBO5.0[91] in which the 5*d* (for Ln) and 6*d* (for An) subshells were included in the valence space. The NBO keyword combination *bndidx*, *dipole*, and *cmo*, as well as the standard NBO output, yielded all of the NBO data presented here. Molecular orbital pictures were generated in VMD.[92]

Scanning Transmission X-ray Spectromicroscopy of Uranium and Aluminum. The scanning transmission X-ray microscope (STXM) at the Advanced Light Source-Molecular Environmental Sciences (ALS-MES) Beamline 11.0.2 is utilized for X-ray absorption near-edge structure (XANES) at the light element thresholds and at the actinide $N_{V,IV}$ ($4d_{5/2,3/2}$) core level edges (700 to 940 eV) downstream of an elliptical polarization undulator (EPU).[44a] The ALS-MES STXM can image and collect XANES spectra from particles with a spatial resolution better than 30 nm from 110 to 2160 eV.[43] The ALS-MES STXM is downstream of the variable angle-included plane grating monochromator that is used routinely to collect Al K-edge XANES data.[93] XANES is a probe of electronic structure that yields both chemical and symmetry (structural) information. XANES spectra are composed of transitions from occupied element-specific electron core levels to unoccupied states.[94] Safety precautions for radioactive STXM investigations require encapsulation of the actinide materials between two thin (100 nm) silicon nitride windows, and this is accomplished by sealing the two silicon nitride windows together with epoxy. The air-sensitive complexes were prepared and sealed

(71) *SAINT: SAX Area-Detector Integration Program*, V6.40; Siemens Industrial Automation Inc.: Madison, WI, 2003.
(72) *XPREP*; Bruker Analytical X-ray Systems Inc.: Madison, WI, 2003.
(73) *SADABS: Bruker-Nonius Area Detector Scaling and Absorption*, v. 2.05; Bruker Analytical X-ray Systems Inc.: Madison, WI, 2003.
(74) Sheldrick, G. M. *SHELXS*; Bruker Analytical X-ray Systems Inc.: Madison, WI, 1995−99.
(75) *XL: Program for the Refinement of X-ray Crystal Structures, Part of the SHELXTL Crystal Structure Determination Package*; Bruker Analytical X-ray Systems Inc.: Madison, WI, 1995−99.
(76) Farrugia, L. J. *J. Appl. Crystallogr.* **1997**, *30*, 565.
(77) Frisch, M. J. et al. *Gaussian 03*, Revision D.01; Gaussian, Inc.: Wallingford, CT, 2004.
(78) Bacskay, G. B. *Chem. Phys.* **1981**, *61*, 385–404.
(79) (a) Becke, A. D. *Phys. Rev. A* **1988**, *38*, 3098–3100. (b) Lee, C. T.; Yang, W. T.; Parr, R. G. *Phys. Rev. B* **1988**, *37*, 785–789.
(80) Perdew, J. P. In *Electronic Structure of Solids*; Ziesche, P., Esching, H., Eds.; Akademie Verlag: Berlin, 1991.
(81) (a) Perdew, J. P.; Burke, K.; Ernzerhof, M. *Phys. Rev. Lett.* **1996**, *77*, 3865–3868. (b) Perdew, J. P.; Burke, K.; Ernzerhof, M. *Phys. Rev. Lett.* **1997**, *78*, 1396–1396.
(82) Stephens, P. J.; Devlin, F. J.; Chabalowski, C. F.; Frisch, M. J. *J. Phys. Chem.* **1994**, *98*, 11623–11627.
(83) Becke, A. D. *J. Chem. Phys.* **1993**, *98*, 5648–5652.
(84) (a) Metz, B.; Stoll, H.; Dolg, M. *J. Chem. Phys.* **2000**, *113*, 2563–2569. (b) Peterson, K. A. *J. Chem. Phys.* **2003**, *119*, 11099–11112.
(85) (a) Dolg, M.; Stoll, H.; Preuss, H. *J. Chem. Phys.* **1989**, *90*, 1730–1734. (b) Cao, X. Y.; Dolg, M. *THEOCHEM* **2002**, *581*, 139–147.
(86) (a) Kuechle, W.; Dolg, M.; Stoll, H.; Preuss, H. *J. Chem. Phys.* **1994**, *100*, 7535. (b) Cao, X. Y.; Dolg, M.; Stoll, H. *J. Chem. Phys.* **2003**, *118*, 487–496. (c) Cao, X.; Dolg, M. *THEOCHEM* **2004**, *673*, 203.
(87) http://www.theochem.uni-stuggart.de/psuedopotentials/.
(88) (a) Hehre, W. J.; Ditchfield, R.; Pople, J. A. *J. Chem. Phys.* **1972**, *56*, 2257. (b) Hariharan, P. C.; Pople, J. A. *Theor. Chim. Acta* **1973**, *28*, 213.
(89) (a) Krishnan, R.; Binkley, J. S.; Seeger, R.; Pople, J. A. *J. Chem. Phys.* **1980**, *72*, 650–654. (b) McLean, A. D.; Chandler, G. S. *J. Chem. Phys.* **1980**, *72*, 5639–5648.
(90) Reed, A. E.; Curtiss, L. A.; Weinhold, F. *Chem. Rev.* **1988**, *88*, 899–926.
(91) Glendening, E. D.; Badenhoop, J. K.; Reed, A. E.; Carpenter, J. E.; Bohmann, J. A. ; Morales, C. M.; Weinhold, F. *NBO 5.0*; Theoretical Chemistry Institute, University of Wisconsin: Madison, WI, 2001 (http://www.chem.wisc.edu/~nbo5).
(92) Humphrey, W.; Dalke, A.; Schulton, K. *J. Mol. Graphics* **1996**, *14*, 1–33.
(93) Tyliszczak, T.; Warwick, T.; Kilcoyne, A. L. D.; Fakra, S.; Shuh, D. K.; Yoon, T. H.; Brown, G. E.; Andrews, S.; Chembrolu, V.; Strachan, J.; Acremann, Y. *Synchrotron Radiation Instrumentation 2003, AIP Conference Proceedings* **2004**, *705*, 1356–1359.
(94) Stohr, J. *NEXAFS Spectroscopy*; Springer-Verlag: Berlin, 2003.

in STXM sample window packages in an Ar inert-atmosphere glovebox. The STXM packages were transferred from the glovebox to the ALS-MES STXM end station in sealed bottles and loaded into the STXM under a back pressure of He. The STXM was then dynamically pumped and backfilled with He to approximately atmospheric pressure. Two different zone plates were used in the STXM, a 30 nm zone plate for the U studies and a 40 nm zone plate for Al studies.

The ALS-MES STXM data collection has been described in detail, and spectra from the complexes were extracted from image stacks (a complete set of registered images collected sequentially at each photon energy of a spectral scan).[95] All spectra were normalized to the incoming flux by integrating over the response from areas without sample particulates. The ALS operated at 500 mA of continuously stored electron beam during the data collection from the complexes.

The energy calibration for the U 4*d* spectrum was referenced to the first absorption maximum of Ne at 867.3 eV. The spatial resolution for the U image and spectrum is 40 nm with an energy resolution of 70 meV. The peak energy assignments for the U 4*d*-edges are estimated at ±40 meV. The U spectrum extracted from the stack had a linear background subtracted. The U spectrum was recorded with an optical density of 1.20 below the edge threshold and 1.42 at maximum, corresponding to an absorption edge jump of 0.22. The final U spectrum was partially smoothed using a five-point routine between the U $4d_{5/2}$ and U $4d_{3/2}$ features only.

The energy scale of the Al K-edge spectra was calibrated to a slightly oxidized Al foil at 1559.0 eV. The spatial resolution for the Al image and spectra is 50 nm with an energy resolution of 250 meV. Spectra were collected from 1550 to 1600 eV as stacks, except for the Al foil which was collected as a line scan. The peak energy assignments for the Al K-edge spectra are estimated at ±125 meV. The Al spectra from the complexes were extracted from stacks, and all spectra had linear backgrounds subtracted. The resultant Al XANES spectrum was normalized to the continuum signal at 1600 eV for comparison. The Al spectra were recorded with the following optical densities before the edge, at maximum, and with absorption edge jumps, respectively [$(Cp^*Al)_4$: 0.28, 1.52, 1.24; $(CpSiMe_3)_3U-AlCp^*$: 0.54, 0.63, 0.09; and Al foil: 1.04, 1.28, 0.24]. The $(Cp^*Al)_4$ spectrum was unsmoothed, whereas the other spectra were smoothed with either a three-point or five-point routine excepting regions with sharp features.

Magnetic Measurements. Finely dispersed powder samples of **1** and **2** were loaded into quartz tubes and embedded in eicosane under an inert atmosphere. The quartz tubes were then sealed under vacuum. DC magnetic susceptibility measurements were collected using a Quantum Design MPMS2 SQUID magnetometer. Measurements were performed at temperatures ranging from 1.8 to 300 K under an applied field of 1 T. The data were corrected for diamagnetic contributions from the core diamagnetism of each sample estimated using Pascal's constants to give $\chi_D = -4.54 \times 10^{-4}$ and -4.60×10^{-4} emu mol^{-1} for **1** and **2**, respectively.

Synthesis of $(CpSiMe_3)_3U-AlCp^*$ (1). The following is a slight modification of our published procedure.[11] To a solution of $(CpSiMe_3)_3U$ (0.87 g, 1.3 mmol) in toluene (15 mL) was added a separate solution of $(Cp^*Al)_4$ (0.22 g, 0.34 mmol) in toluene (15 mL) which had been cooled to −78 °C. The mixture was allowed to warm with the cold bath to room temperature while stirring over 12 h. At this point the solution remained green with a yellow precipitate from unreacted soluble $(CpSiMe_3)_3U$ and relatively insoluble $(Cp^*Al)_4$. After the mixture stirred at 60 °C for 2 h, the color changed from dark green to dark red as the yellow precipitate disappeared, and the solution was cooled to room temperature. The volatile components were removed *in vacuo*, and the solid was extracted with pentane (20 mL). Cooling to −80 °C over 24 h and storage for an additional 2 d afforded the product as X-ray quality dark red blocks (0.41 g, 39%). ^{1}H NMR (500 MHz, d_8-toluene, 19.2 °C): δ −6.89 (s, 15 H, $C_5(CH_3)_5$, $\Delta\nu_{1/2} = 4.58$ Hz), −11.95 (s, 27 H, $SiMe_3$, $\Delta\nu_{1/2} = 2320$ Hz), −18.95 (s, 6 H, ring H, $\Delta\nu_{1/2} = 78.6$ Hz). ^{1}H NMR (500 MHz, d_8-toluene, 82.7 °C): δ 3.66 (s, 6 H, ring H, $\Delta\nu_{1/2} = 45.5$ Hz), −4.50 (s, 15 H, C_5Me_5, $\Delta\nu_{1/2} = 13.5$ Hz), −11.10 (s, 27 H, $SiMe_3$, $\Delta\nu_{1/2} = 24.9$ Hz), −14.85 (s, 6 H, ring CH, $\Delta\nu_{1/2} = 22.3$ Hz). IR (cm^{-1}): 1244 (m), 1174 (m), 1098 (w), 1038 (m), 901 (m), 832 (s), 770 (m), 723 (w), 687 (w), 637 (w), 625 (w), 584 (w), 460 (m), 418 (w). MS (EI, 70 eV) *m/z*: 734 [$M^+ - SiMe_3$] (predicted isotope envelope was observed), 720 [$M^+ - (C_5H_4 + Al)$], 649 [$M^+ - Cp^*Al$]. Anal. Calcd for $C_{34}H_{54}Si_3UAl$: C, 50.29; H 6.70. Found: C, 49.75; H, 6.84. Mp = 115.5−116 °C.

$(CpSiMe_3)_3U-GaCp^*$ (2). To a solution of $(CpSiMe_3)_3U$ (1.2 g, 1.9 mmol) in pentane (5 mL) was added a solution of Cp*Ga (0.38 mg, 1.9 mmol) in pentane (5 mL). The reaction went to completion immediately as evidenced by a color change from green to dark green. Storage at −80 °C for several days afforded the product as X-ray quality dark green blocks (1.4 g, 90%). ^{1}H NMR (500 MHz, d_8-toluene, 21.4 °C): δ 4.31 (s, 6 H, ring H, $\Delta\nu_{1/2} = 46.4$ Hz), −1.16 (s, 15 H, C_5Me_5, $\Delta\nu_{1/2} = 9.73$ Hz), −14.75 (s, 27 H, $SiMe_3$, $\Delta\nu_{1/2} = 26.1$ Hz), −19.18 (s, 6 H, ring H, $\Delta\nu_{1/2} = 22.5$ Hz). IR (cm^{-1}): 1417 (w) 1362 (w), 1308 (w), 1245 (s), 1174 (m), 1089 (w), 1038 (m), 988 (w), 902 (m), 837 (s), 763 (s), 688 (w), 625 (w), 514 (w), 421 (w). MS (EI, 70 eV) *m/z*: 649 [$M^+ - Cp^*Ga$]. Anal. Calcd for $C_{34}H_{54}Si_3UGa$: C, 47.77; H 6.37. Found: C, 47.48; H, 6.42. Mp = 95−96 °C.

$(CpSiMe_3)_3Nd$. $(CpSiMe_3)K$ (2.2 g, 12 mmol) was dissolved in warm toluene (20 mL), and the solution was added to a suspension of $NdCl_3$ (1.0 g, 4.0 mmol) in toluene (20 mL). The mixture was stirred at reflux for 24 h. Volatiles were removed by evaporation *in vacuo*, and the solid residue was extracted with pentane (2 × 50 mL). The combined light yellow-green extracts were concentrated to 20 mL. Storage at −80 °C for 24 h afforded the product as large yellow-green needles (1.5 g, 67%). ^{1}H NMR (500 MHz, d_8-toluene, 21.0 °C): δ 28.42 (s, 6 H, ring H, $\Delta\nu_{1/2} = 42.7$ Hz), −2.83 (s, 6 H, ring H, $\Delta\nu_{1/2} = 36.0$ Hz), −15.14 (s, 27 H, $SiMe_3$, $\Delta\nu_{1/2} = 12.8$ Hz). ^{13}C NMR (130 MHz, C_6D_6, 22.0 °C): δ 258.2, 256.2, 236.5, −17.2. IR (cm^{-1}): 1363 (m), 1311 (w), 1248 (s), 1178 (m), 1092 (w), 1041 (m), 948 (w), 903 (m), 886 (w), 832 (s), 771 (s), 751 (m), 687 (w), 629 (m), 535 (w). Anal. Calcd for $C_{24}H_{39}Si_3Nd$: C, 51.84; H, 7.07. Found: C, 51.70; H, 7.34. Mp = 72−73 °C.

NMR Observation of $(CpSiMe_3)_3Nd-AlCp^*$ (3). A suspension of powdered $(Cp^*Al)_4$ (6.2 mg, 9.6 μmol) in d_8-toluene (0.25 mL) was added to a solution of $(CpSiMe_3)_3Nd$ (21 mg, 38 μmol) in d_8-toluene (0.25 mL) and sealed under N_2 in a J-Young NMR tube. The sample was heated to 82.8 °C inside the probe of a DRX-500 NMR spectrometer, given approximately 30 min to reach equilibrium, and ^{1}H and ^{27}Al NMR spectra were collected. While cooling to −33.2 °C, a spectrum was collected approximately every 10 °C, allowing 15 min at each temperature adjustment for the system to reach equilibrium. ^{1}H NMR (500 MHz, d_8-toluene): the spectra are summarized in Table S7 in the Supporting Information. ^{27}Al NMR (130 MHz, d_8-toluene): no signal detected between ± 1400 ppm.

NMR Observation of $(CpSiMe_3)_3Nd-GaCp^*$ (4). A solution of Cp*Ga (*n* molar equivalents) in d_8-toluene (0.25 mL) was added to a solution of $(CpSiMe_3)_3Nd$ (20 mg, 36 μmol) in d_8-toluene (0.25 mL) and sealed under N_2 in a J-Young NMR tube. The value of *n* is chosen to achieve the desired molar fraction (x_{NdGa}) of product in solution; limit behavior is reached above $n = 10$. ^{1}H NMR (500 MHz, d_8-toluene): the spectra are summarized in Table S8 in the Supporting Information.

Determination of Thermodynamic Parameters for 2 and 4. A standard procedure was followed based on a slight modification of the literature method.[17c] For example, a solution of $(CpSiMe_3)_3U$ (20 mg, 31 μmol) in d_8-toluene (0.25 mL) was combined with a solution of *n* molar equiv of Cp*Ga in d_8-toluene (0.25 mL) under N_2 in a J-Young NMR tube, producing an immediate reaction. ^{1}H

(95) Hitchcock, A. P. *aXis*, version 17; McMaster University: Hamilton, Ontario, Canada, 2008.

NMR spectra were collected at 10 °C intervals between 21.5 and 72.0 °C for **2** and −33.2 and 19.2 °C for **4**, allowing 15 min between steps. Separate samples were prepared for each value of *n*. The $CpSiMe_3$ resonances were not shifted upon adding additional equivalents of Cp*Ga once limit behavior was reached ($n = 8.77$ for **2** and 10.3 for **4**). The spectra are summarized in Tables S4 and S9 for **2** and **4**, respectively, and thermodynamic parameters ΔH and ΔS are given in Tables S5 and S10.

No significant difference was observed in the thermodynamic parameters for **2** by performing the ^{1}H NMR experiments between −33.2 and 19.2 °C. Of the three $CpSiMe_3$ resonances observed for **2**, only the downfield ring and $SiMe_3$ protons confirmed that formation of **2** is exothermic; for consistency, the downfield ring proton resonance was used for the thermodynamic analysis. For unknown reasons, the upfield resonance assigned to ring protons did not behave as expected for an exothermic reaction (see Figure S7 in Supporting Information). Interestingly, all three $CpSiMe_3$ resonances observed for **4** confirmed that its formation is exothermic, and all were used for the thermodynamic analysis.

Reaction of 1 and 2 with Small Molecules. A standard procedure was followed, for example: a solution of **1** (20 mg, 12 μmol) in d_8-toluene (0.25 mL) was combined with a solution of 1 equiv of ligand (L) in d_8-toluene (0.25 mL) under N_2 in a J-Young NMR tube. In the case of L = CO and CO_2, the metallocene was dissolved in d_8-toluene (0.5 mL), sealed in a J-Young NMR tube, degassed on a Schlenk line, and introduced to the gas (1 atm, *ca.* 4 equiv). After at least 10 min, a ^{1}H NMR spectrum was collected. These results are summarized in Table 2.

Competition Reactions. The literature procedure[17c] was followed for the **2/4** system: a solution of **2** (17 mg, 20.0 μmol) in d_8-toluene (0.25 mL) was combined with a solution of $(CpSiMe_3)_3Nd$ (11 mg, 20.0 μmol) in d_8-toluene (0.25 mL) under N_2 in a J-Young NMR tube. After at least 10 min, a ^{1}H NMR spectrum was collected. The experiment was repeated four times on independent samples, and results are summarized in Table 1. Samples were prepared in a similar fashion for the **1/3** system, and relative concentrations of **1** and **3** were determined by integration of the peaks corresponding to the independent Cp* proton resonances in **1** and **3**. Monomeric Cp*Al does not persist in detectable concentrations at room temperature;[28] therefore we assume the intensity of these peaks derives entirely from the presence of **1** or **3**.

Acknowledgment. We thank Drs. R. Andersen, R. Bergman, L. Maron, and W. Lukens for helpful discussions, as well as Drs. F. Hollander, A. DiPasquale, and M. Mulvihill for assistance with measurements, and the DOE for financial support of the preliminary aspects of this work through the LBNL-LDRD program. Parts of this work (T.T., D.K.S.) and the ALS were supported by the Director, Office of Science, Office of Basic Energy Sciences and by the Division of Chemical Sciences, Geosciences, and Biosciences of the U.S. Department of Energy at LBNL under Contract No. DE-AC02-05CH11231. R.C. was supported by the Laboratory Directed Research and Development Program at LBNL. Molecular modeling was performed at the UC Berkeley Molecular Graphics and Computation Facility, directed by Dr. K. Durkin and operated with equipment funds from NSF Grant CHE-0233882 and donations from Dell.

Supporting Information Available: Crystallographic data for all structures (CIF). Complete author list for ref 77. Full ^{1}H NMR chemical shift and line-width details for NMR spectroscopy experiments in both table and chart form. Positional coordinates, energies, and M−E bond lengths (where applicable) for all calculated structures. This material is available free of charge via the Internet at http://pubs.acs.org.

JA904565J